

NASA TECHNICAL NOTE



NASA TN D-4316

NASA TN D-4316



TECH LIBRARY KAFB, NM

LOAN COPY: RETURN TO
AFWL (WLIL-2)
KIRTLAND AFB, N MEX

SUBSONIC AND TRANSONIC FLUTTER AND FLOW INVESTIGATIONS OF THE T-TAIL OF A LARGE MULTIJET CARGO AIRPLANE

*by Maynard C. Sandford, Charles L. Rublin,
and E. Carson Yates, Jr.*

*Langley Research Center
Langley Station, Hampton, Va.*

TECH LIBRARY KAFB, NM



0131346

SUBSONIC AND TRANSONIC FLUTTER AND FLOW INVESTIGATIONS
OF THE T-TAIL OF A LARGE MULTIJET CARGO AIRPLANE

By Maynard C. Sandford, Charles L. Ruhlin,
and E. Carson Yates, Jr.

Langley Research Center
Langley Station, Hampton, Va.

NATIONAL AERONAUTICS AND SPACE ADMINISTRATION

For sale by the Clearinghouse for Federal Scientific and Technical Information
Springfield, Virginia 22151 - CFSTI price \$3.00

SUBSONIC AND TRANSONIC FLUTTER AND FLOW INVESTIGATIONS
OF THE T-TAIL OF A LARGE MULTIJET CARGO AIRPLANE

By Maynard C. Sandford, Charles L. Ruhlin,
and E. Carson Yates, Jr.
Langley Research Center

SUMMARY

Flutter and flow studies of the T-tail of a large multijet cargo airplane have been conducted in the Langley transonic dynamics tunnel at Mach numbers up to 1.08. The tail and aft fuselage of the model employed were geometrically, dynamically, and elastically scaled, whereas only the mass and stiffness characteristics of the forward fuselage, wings, and nacelles were simulated. The flutter studies included variations in fin-spar stiffness, stabilizer-pitch-actuator stiffness, rotational stiffnesses of elevators and rudder, as well as small variations in stabilizer incidence angle. Flow studies were initiated to reduce areas of separated flow in the vicinity of the fin-stabilizer juncture and included the use of vortex generators and fences, as well as modifications to the bullet-fairing shape.

The results indicated that for a configuration with a weaker-than-design fin spar, the antisymmetric flutter boundary had a transonic dip amounting to a 41-percent reduction in dynamic pressure from the low-speed value, the minimum occurring near Mach number 0.7. For the design configurations, no flutter occurred within the Mach number and dynamic-pressure ranges investigated. Separated flow over the fin and stabilizer was alleviated by the use of vortex generators, but flow over the aft portion of the bullet fairing remained separated.

INTRODUCTION

The structural design of T-tails for high-performance aircraft is often significantly influenced by flutter-clearance requirements; thus, the pertinent flutter boundaries must be accurately known if excessive weight is to be avoided. Since critical flight conditions for the occurrence of flutter usually appear in the transonic range, it is imperative that the level of the transonic flutter speed be reliably estimated early in the design process. Because analytical methods are least reliable for the transonic range, the designer usually obtains preliminary information of this type from flutter trend studies conducted in the low subsonic range together with an estimate of the magnitude of the characteristic transonic dip based on published experimental data. However, much of the existing

information on T-tail flutter is unpublished, and most of the published experimental studies (refs. 1 to 8, for example) have not covered a sufficient Mach number range to show the magnitude of the transonic dip in the antisymmetric flutter speed. One exception is reference 9 which does show the extent of the dip.

This paper presents the results of some limited subsonic and transonic flutter experiments which were initiated primarily to demonstrate flutter margins for the T-tail of a large multijet cargo airplane. Flutter experiments with an earlier design for this T-tail (ref. 10) employed the same basic model as the present investigation and included extensive variations in flow conditions as well as in several structural parameters but produced little antisymmetric-flutter data. Therefore, in the present investigation a weakened-fin-spar configuration was studied in addition to the current design configuration in an attempt to determine transonic antisymmetric flutter characteristics and the depth of the transonic dip in the antisymmetric flutter speed.

Early in the present investigation extensive flow separation was detected in the vicinity of the fin-stabilizer juncture. Since the associated effect on tail load distributions could influence flutter behavior as well as aerodynamic characteristics, flow studies were conducted to determine methods of reducing the areas of separated flow. The effectiveness of several model modifications employed for this purpose is indicated herein.

The experiments were conducted in the Langley transonic dynamics tunnel in air at Mach numbers up to 0.90 or in Freon-12 (dichlorodifluoromethane) at Mach numbers up to 1.08.

SYMBOLS

b	stabilizer semichord at plane of symmetry, ft (m)
EI	bending stiffness, lb-in ² (kN-m ²)
f	flutter frequency, cps
f _e	natural frequency of elevator rotation, cps
f _i	natural frequency of ith antisymmetric structural vibration mode, cps
f _r	natural frequency of rudder rotation, cps
f _θ	uncoupled pitch frequency of horizontal tail, cps
g	structural damping coefficient

GJ	torsional stiffness, lb-in ² (kN-m ²)
I _{ea}	mass moment of inertia of stabilizer section or fin section about its elastic axis, slug-ft ² (kg-m ²)
I _{h_l}	mass moment of inertia of elevator or rudder about its hinge line, slug-ft ² (kg-m ²)
I _θ	mass moment of inertia of horizontal tail (including elevators and bullet fairing) in pitch about horizontal-tail pivot axis, slug-ft ² (kg-m ²)
I _ψ	mass moment of inertia of horizontal tail (including elevators and bullet fairing) in yaw about a vertical axis through intersection of fin elastic axis and stabilizer horizontal plane, slug-ft ² (kg-m ²)
I _φ	mass moment of inertia of horizontal tail (including elevators and bullet fairing) in roll about intersection of stabilizer horizontal plane and plane of symmetry, slug-ft ² (kg-m ²)
M	Mach number
m _e	total mass of empennage, slugs (kg)
m _h	total mass of horizontal tail (including elevators and bullet fairing), slugs (kg)
m _v	total mass of vertical tail (including rudder), slugs (kg)
q	dynamic pressure, lb/sq ft (kN/m ²)
N _{Re}	Reynolds number per unit length, ft ⁻¹ (m ⁻¹)
S _{ea}	mass unbalance of stabilizer section or fin section about its elastic axis, slug-ft (kg-m)
S _{h_l}	mass unbalance of elevator or rudder about its hinge line, slug-ft (kg-m)
V	free-stream velocity, ft/sec (m/s)

v	volume of a conical frustum having horizontal-tail root chord as base diameter, horizontal-tail tip chord as upper diameter, and horizontal-tail semi-span as height, 2.68 cu ft (0.0759 m ³)
α_t	angle of attack of horizontal tail, deg
η_{ea}	distance along elastic axis (spar center line) of fin or stabilizer measured from elastic-axis root, fraction of elastic-axis length
η_{hl}	distance along hinge line of rudder or elevators measured from control surface root, fraction of hinge-line length
μ	mass ratio of horizontal tail, $m_h/2\rho v$
ρ	test-medium density, slugs/ft ³ (kg/m ³)

Subscript:

o nominal design condition

Abbreviations:

BL	buttock line, in. (cm)
FS	fuselage station, in. (cm)
WL	water line, in. (cm)

MODEL

General Description

The T-tail and aft fuselage of the model used in this investigation (figs. 1 and 2), were geometrically, dynamically, and elastically scaled so that in freon, the Mach number, mass ratio, and reduced frequency were simulated for the subject airplane in the atmosphere. The mass and stiffness distributions of the forward fuselage, as well as the overall mass and elastic properties of the wings and nacelles, were also represented, although these components were not geometrically scaled. Specifically, overall vibrational characteristics of the airplane wing with multiple engine pods were represented by a simulated wing with a single, simulated nacelle at the tip. This model was basically

the same as that of reference 10 except for changes in stabilizer planform and stiffness, fin-stabilizer joint stiffness, wing mass, and pylon stiffness. In addition, during the present investigation some modifications in the shape of the bullet fairing were made and vortex generators were installed in order to improve the flow in the vicinity of the fin-stabilizer juncture. The geometric properties given in table I are pertinent to all model configurations although several interchangeable structural members were employed in order to vary component stiffnesses. Table I also includes geometric properties of the model of reference 10 for comparison.

Construction

Stabilizer and fin. - The stabilizer and fin were of a spar-and-pod construction (figs. 1(b) and 1(c)). Single box spars provided the required stiffness distributions in bending and torsion. The pods were constructed of pine and balsa ribs covered with sheet balsa and doped silk span. Lead weights were installed in the pods to yield the required mass, center of gravity, and moment of inertia. The gaps between the pods were aerodynamically closed with sponge rubber.

The stabilizer was attached to the vertical tail by two aluminum bracket arms with ball bearing pivots which fitted on a lateral shaft mounted at the top of the fin spar. (See fig. 1(d).) The fin-stabilizer joint area was enclosed by a bullet fairing of balsa covered with doped silk. (See figs. 1(a) and 1(b).) The stabilizer could be trimmed in pitch relative to the fin by means of a jack screw driven through an articulated shaft by an electric motor located in the fuselage. (See figs. 1(c) and 1(d).) The articulated shaft was connected to the stabilizer with a U-shaped metal spring which simulated the stiffness of the pitch-trim actuator.

Control surfaces. - The elevator and rudder spars were constructed of balsa covered with thin sheet metal. (See figs. 1(b) and 1(c).) The contours were built up of pine ribs covered with doped Japanese tissue (rudder) or sheet balsa and doped silk span (elevators). Each elevator was fully mass balanced, but the rudder was not. Left and right elevators were flexibly interconnected in order to simulate carry-through stiffnesses.

Fuselage. - The fuselage was of spar-and-pod construction. The forward fuselage, which did not simulate the airplane geometrically, was composed of solid balsa pods which formed a cylinder around the spar. The geometrically scaled aft-fuselage pods were built of plywood and magnesium bulkheads covered with sheet balsa (fig. 1(a)). Two rotating-unbalanced-mass shakers were mounted inside the nose of the fuselage spar in order to excite the vertical and lateral modes of the model.

Wings and nacelles. - Each simulated wing panel consisted of a solid, aluminum-alloy rectangular-cross-section beam which was bolted onto an H-fitting mounted on top of the fuselage spar. Balsa aerodynamic fairings were attached to the leading and trailing

edges of the wing beams (figs. 1(a) and 1(d)), and the entire simulated wing was wrapped with sheet lead. The simulated nacelles were aluminum-alloy beams with large lead masses attached to the forward end. These nacelles were attached to the outboard ends of the wing beams by I-beam pylons which were streamlined with balsa fairings.

Mounting cage.- The mounting cage (figs. 1(a) and 1(d)) had four lengths of 0.20-inch-diameter (0.51-cm) music wire which were rigidly attached to the fuselage about the center of gravity and extended symmetrically above and below the center of gravity. At their extremities, these four vertical wires were attached to two exposed plates which are nominally parallel to the free stream. The upper plate was streamlined with balsa fairings. The model was supported in the tunnel by mounting cables which were attached to the two plates of the mounting cage.

Further details of the model construction may be found in reference 10.

Instrumentation

Wire strain gages were mounted near the root of the stabilizer and fin spars to indicate deflections in bending and torsion. Small magnetic-induction pickups measured rotational motion of the elevators and the rudder. Strain gages were attached to the aft-fuselage spar to indicate deflections in vertical bending, lateral bending, and torsion. An inclinometer and an accelerometer mounted near the model center of gravity measured the fuselage pitch angle and vertical translational motion, respectively. Another accelerometer installed in the right nacelle gave an indication of nacelle vertical motion. Tufts of yarn were attached to the surfaces of the vertical and horizontal tail for flow visualization.

Physical Properties

Mass and stiffness.- A summary of the model configurations and their mass and stiffness properties is given in tables II to IV and in figure 3. (See also ref. 10.) For simplicity, the model configurations have been given coded designations. (See table II.) In this code, a letter D indicates the design configuration, and a letter W indicates a configuration with a weakened fin spar. The first number designates the pitch spring used, and the last number indicates variations in control rotational stiffness, bullet-fairing shape, or vortex-generator configuration.

Natural frequencies and nodal patterns.- Measured symmetric- and antisymmetric-mode natural frequencies are presented in table V for the complete model mounted in the tunnel and for the cantilevered empennage. Nodal patterns shown in figures 4 to 6 are for the principal modes indicated in table V. Complete vibrational surveys were performed on the basic model configurations D and W. Brief frequency surveys were made before and after every run to check for possible model damage.

APPARATUS AND TESTS

Tunnel and Mount System

This investigation was conducted in the Langley transonic dynamics tunnel which has a 16-foot-square (4.88-m) test section (with cropped corners) and is a return-flow, variable-pressure, slotted-throat wind tunnel (ref. 11). It is capable of operation at stagnation pressures from near vacuum to slightly above atmospheric and at Mach numbers from 0 to 1.2. Mach number and dynamic pressure can be varied independently with either air or freon used as a test medium. The tunnel is equipped with a quick-opening bypass valve (ref. 11) which can be opened when flutter occurs in order to reduce rapidly the dynamic pressure in the test section.

The model was supported in the tunnel by cables which were attached to the upper and lower end plates of the mounting cage previously described. (See fig. 1(d) and ref. 10.) Springs in cables 1 and 2 (fig. 1(d)) allowed freedom of the model in vertical translation, whereas flexure of the four vertical wires of the mounting cage permitted freedom in roll, pitch, and yaw as well as in lateral translation. A continuous cable (cable 7) extended laterally forward from the model to reduce the drag loads on the mounting cage and to alleviate a Dutch roll tendency of the model. This cable passed through the tunnel side walls and was supported by pulleys external to the test section.

Tests

Equipment.- During the tests, strain-gage and accelerometer signals from the model were continuously recorded on direct readout recorders and on magnetic tape. Visual records of model and tuft behavior were provided by high-speed motion pictures taken from the sides and from the rear. Tunnel conditions, such as tunnel stagnation and static pressures and stagnation temperature, were automatically digitized and printed. For tests in freon, the purity of the freon was determined with a meter which sensed the variation of the magnetic susceptibility of the oxygen content of the testing medium. The purity of the freon varied during the tests between 90 and 98 percent by volume (97.4 to 99.6 percent by weight).

Procedure.- Prior to testing, the model angle of attack and the stabilizer incidence angle were nominally set at 0° . During one of the tests, the stabilizer incidence angle was remotely varied in order to vary the angle of attack of the horizontal tail. In addition, it was occasionally necessary to adjust the stabilizer incidence in order to relieve excessive static loads on the stabilizer.

Most of the tests in freon were limited to $M \leq 0.90$ which was approximately the design limit for the airplane. Although the model in air at the higher Mach numbers did not scale to the airplane values of mass ratio and reduced frequency, the tests in air were

extended to $M = 0.90$ in an attempt to obtain flutter data for direct comparison with corresponding results in freon and with previous low-speed tests in air. Investigations with control-surface freedoms were extended to very low dynamic pressures and Mach numbers because calculations and previous low-speed tests indicated that control-surface instabilities would be most likely to occur in this region.

The test procedure was essentially the same for tests in air and in freon. This procedure is illustrated in figure 7 by a typical operating path described in terms of dynamic pressure as a function of Mach number. The operating sequence shown was employed to cover the desired ranges of dynamic pressure and Mach number in minimum running time. During some of the early tests, the model was occasionally excited both laterally and vertically at frequencies up to 20 cps by the shakers built into the fuselage nose. This practice was discontinued because at the higher dynamic pressures the model response to tunnel turbulence became greater than the response to shaker excitation. When flutter was observed, the tunnel bypass valve was opened and the tunnel fan speed was decreased to reduce rapidly the dynamic pressure in the test section.

RESULTS AND DISCUSSION

Flutter Studies

Previous experiments with an earlier design of this T-tail (ref. 10), as well as flutter calculations for the current design, indicated that for the design stiffness condition symmetric flutter would occur at lower dynamic pressure than antisymmetric flutter. Therefore, in addition to the current design configuration D, a weakened-fin-spar configuration W was studied in an attempt to determine transonic antisymmetric-flutter characteristics without encountering symmetric flutter. A compilation of test results are presented in table VI.

Configuration W. - Configuration W was to have been tested in air and then in freon to evaluate the effect on antisymmetric flutter of varying the mass ratio. However, destruction of the model during the air studies precluded further tests. For this weakened-fin-spar configuration only one flutter point was obtained, as shown in figure 7 at $M = 0.698$ and $q = 100.6 \text{ lb/sq ft}$ (4.817 kN/m^2). The flutter motion was antisymmetric (primarily fin bending and torsion) and quickly destroyed the entire empennage. The location of this flutter point relative to the adjacent no-flutter points (fig. 7) indicates that the flutter point is at or very near the bottom of the characteristic transonic dip. It is evident from figure 7 that the bottom of the dip could not occur at a much higher Mach number because of the presence of the no-flutter points. Furthermore, the low Mach number at which flutter occurred indicates that it is very unlikely that the minimum could be at a much lower Mach number.

The low-speed model flutter point shown in figure 7 was obtained with a dynamically and elastically scaled model having the same shape and size as that of the present investigation. Flutter data (unpublished) obtained with this model were related to results of the high-speed model by means of the flutter-speed index $\frac{V}{b(2\pi f_2)\sqrt{\mu}}$ as indicated in the appendix. Comparison of this adjusted low-speed flutter point with the high-speed data provides an indication of the depth of the transonic dip as well as a reasonable estimate of the flutter boundary itself. This comparison shows a transonic dip in flutter dynamic pressure amounting to a 41-percent reduction from the low-speed value. In contrast, the model of reference 9, which had 15° dihedral and a more highly swept stabilizer, had a transonic dip amounting to about 24-percent reduction, the minimum occurring at about $M = 0.77$.

Configurations D.- For design configurations D, no flutter occurred within the Mach number and dynamic-pressure ranges covered (fig. 8). These design configurations included reductions in control stiffnesses to simulate control-actuator failures. (See table II.) In the present studies, the stabilizer angles of attack α_t were limited by the test apparatus and by structural loads imposed on the model and, therefore, did not include the higher positive angles at which the airplane is capable of operating. It should be noted that typical behavior for T-tails (for example, ref. 1) indicates significant reduction in the antisymmetric-flutter dynamic pressure as tail angle of attack increases. Low-speed tests of the present configuration have shown a dynamic-pressure reduction of about 13 percent per degree for angles of attack near zero.

Flow Studies

Tuft studies of the initial configurations (W1-1) revealed extensive areas of separated flow over the aft portion of the fin-stabilizer juncture. As shown in figure 9(a) (right side), the separated flow covered a significant region of the fin and rudder at the higher Mach numbers. Although this separated flow may have some effect on antisymmetric flutter, it should have no appreciable effect on symmetric flutter such as that observed in reference 10. Most of the separated flow over the fin and stabilizer was alleviated by use of vortex generators (fig. 9(a)). Boattailing of the bullet fairing (fig. 9(b)) accomplished a little additional improvement. However, the addition of several configurations of fences or faired fences to the bullet fairing (for example, fig. 9(b)) produced no further improvement, and flow over the aft portion of the bullet remained separated.

CONCLUSIONS

Flutter and flow studies of a geometrically, dynamically, and elastically scaled model of the T-tail of a large multijet cargo airplane have been conducted in the Langley

transonic dynamics tunnel at Mach numbers up to 1.08. The results indicate the following conclusions:

1. For a configuration with a weaker-than-design fin spar, the transonic dip in the antisymmetric flutter boundary amounted to a 41-percent reduction in dynamic pressure from the low-speed value, the minimum occurring near a Mach number of 0.7.

2. For the design configurations, no flutter occurred within the Mach number and dynamic-pressure ranges covered. These design configurations included reductions in control stiffnesses to simulate control actuator failures. However, because of the limitations of the test apparatus and model structure, the full range of tail angle of attack for the airplane was not investigated.

3. Extensive flow separation in the vicinity of the fin-stabilizer juncture was alleviated over the fin and stabilizer by the use of vortex generators. However, attempts to eliminate separation over the aft portion of the bullet fairing by modifications to its shape or by the addition of fences proved unsuccessful.

Langley Research Center,
National Aeronautics and Space Administration,
Langley Station, Hampton, Va., July 14, 1967,
126-14-02-03-23.

APPENDIX

BASIS FOR LOW-SPEED ANTISYMMETRIC FLUTTER POINT

Data (unpublished) for the low-speed antisymmetric flutter point (fig. 9) were obtained in a low-speed wind tunnel during flutter tests of a dynamically and elastically scaled model having the same shape and size as that of the present investigation. The two models were similarly constructed and had similar scaled physical properties. For example, for both models the stabilizer spar stiffness was about three-quarters of the scaled design level, and the fin spar stiffness was slightly less than one-half the scaled design level. Some further similarities between overall physical properties for the two models are shown in the following table along with pertinent test conditions:

Model property or test condition	Low-speed model	High-speed model (configuration W1-2)
EI/GJ for fin spar	0.916	0.900
m_v/m_h	1.030	0.912
$I_\theta/m_h b^2$	0.416	0.458
$I_\psi/m_h b^2$	3.18	3.03
$I_\phi/m_h b^2$	2.96	2.78
f_1/f_2 (i.e., $\frac{\text{Fin bending}}{\text{Fin torsion}}$)	0.594	0.573
f_3/f_2 (i.e., $\frac{\text{Stabilizer roll}}{\text{Fin torsion}}$)	1.142	1.200
Model attitude	Upright and inverted	Upright
α_t , deg.	0	-0.3
M	0.13	0.698
μ	18.9	103.0
$\frac{V}{b(2\pi f_2)\sqrt{\mu}}$	*2.172	1.740
f/f_2	*0.879	0.805

*Average values for upright and inverted attitudes.

APPENDIX

The flutter point for the low-speed model was related to that for the high-speed model on the basis of the flutter-speed index $\frac{V}{b(2\pi f_2)\sqrt{\mu}}$ with small adjustments for differences in horizontal-tail angle of attack α_t and mass ratio μ . Adjustment of the low-speed flutter point for the 0.3° difference in α_t was based on low-speed test results and amounted to a 1.8-percent increase in flutter speed. Although the difference in mass ratio is large, flutter calculations for low Mach numbers have shown relatively little sensitivity to variations in μ at least in the range of present interest. On the basis of these calculations, the adjustment of the low-speed flutter point for mass ratio amounted to a 2.5-percent increase in flutter speed. The adjusted flutter dynamic pressure shown in figure 7 for the low-speed model was therefore obtained from

$$\begin{aligned}
 q_{\text{low-speed model}} &= \frac{1}{2} \left\{ \left[\frac{V}{b(2\pi f_2)\sqrt{\mu}} \right]_{\text{low-speed model}} \left[b(2\pi f_2) \sqrt{\frac{m_h}{2v}} \right]_{\text{high-speed model}} (\alpha_t, \text{adjustment}) (\mu \text{ adjustment}) \right\}^2 \\
 &= \frac{1}{2} [(2.172)(8.148)(1.018)(1.025)]^2 \\
 &= 170.5 \text{ lb/sq ft} \quad (8.164 \text{ kN/m}^2)
 \end{aligned}$$

A corresponding adjustment of the low-speed flutter-frequency ratio yields $f/f_2 = 0.820$.

REFERENCES

1. Baldock, J. C. A.: The Determination of the Flutter Speed of a T-tail Unit by Calculations, Model Tests and Flight Flutter Tests. Rep.221, AGARD, North Atlantic Treaty Organization (Paris), Oct. 1958.
2. Land, Norman S.; and Fox, Annie G.: An Experimental Investigation of the Effects of Mach Number, Stabilizer Dihedral, and Fin Torsional Stiffness on the Transonic Flutter Characteristics of a Tee-Tail. NASA TN D-924, 1961. (Supersedes NACA RM L57A24.)
3. Haviland, George P.: Wind-Tunnel Tests of a "Tee" Tail Flutter Model. Tech. Note WCLS 52-21, U.S. Air Force; Oct. 1952.
4. Pengelley, C. D.; Wilson, L. E.; Epperson, T. B.; and Ransleben, G. E., Jr.: Flutter Characteristics of a T-Tail. WADC Tech. Rep. 52-162 (Contract No. AF 33(038)-18404), Wright Air Dev. Center, U.S. Air Force, Nov. 1954.
5. Goldman, R. L.: Flutter of T-Tails With Dihedral. ER 8205, The Martin Co., 1957.
6. Wasserman, Lee S.: Flutter Research of a T-Tail at Transonic Speeds. WADC Tech. Rep. 58-210 (ASTIA Doc. No. AD 303424), U.S. Air Force, Dec. 1958.
7. Anon.: Vibration and Flutter Studies, Models YP6M-1 and P6M-2. Vol. II - Low Speed Tail Flutter Model. ER 9204-II, The Martin Co., Nov. 1957.
8. Fotieo, G.; and Kachadourian, George: Model YP6M-1 Flutter Analysis and Methods and Flutter Model Report. ER 6248, The Martin Co., Mar. 1955.
9. Stahle, C. V.: Transonic Effects on T-Tail Flutter. RM-24, The Martin Co., Feb. 1959.
10. Ruhlin, Charles L.; Sandford, Maynard C.; and Yates, E. Carson, Jr.: Wind-Tunnel Flutter Studies of the Sweptback T-Tail of a Large Multijet Cargo Airplane at Mach Numbers to 0.90. NASA TN D-2179, 1964.
11. Yates, E. Carson, Jr.; Land, Norman S.; and Foughner, Jerome T., Jr.: Measured and Calculated Subsonic and Transonic Flutter Characteristics of a 45° Sweptback Wing Planform in Air and in Freon-12 in the Langley Transonic Dynamics Tunnel. NASA TN D-1616, 1963.

TABLE I.- GEOMETRIC PROPERTIES OF MODEL

	Present model	Model ^a of reference 10
Horizontal tail:		
Stabilizer with elevator:		
Aspect ratio	5.22	5.21
Sweepback angle of quarter-chord line, deg	25	
Taper ratio	0.37	
Airfoil section (streamwise).	NACA 64A010	
Dihedral angle, deg	0.0	
Area, sq ft (m ²).	5.96 (0.554)	6.74 (0.626)
Mean aerodynamic chord, ft (m)	1.148 (0.3499)	1.217 (0.3709)
Span, ft (m)	5.57 (1.70)	5.92 (1.80)
Elastic-axis location, fraction of horizontal-tail chord (streamwise).	0.40	0.41
Length along elastic axis, ft (m)	3.01 (0.917)	3.21 (0.978)
Elevator:		
Spanwise location, fraction of stabilizer semispan, at -		
Root	0.0664	0.0625
Tip	1.000	
Chordwise location, fraction of horizontal-tail chord (streamwise), at -		
Leading edge	0.724	
Trailing edge	1.000	
Hinge axis, fraction of horizontal-tail chord (streamwise)	0.750	
Exposed area, fraction of horizontal-tail area	0.23	
Horizontal-tail pivot axis, fraction of horizontal-tail chord at root (streamwise)	0.602	0.606
Vertical tail:		
Fin with rudder:		
Aspect ratio	1.24	
Sweepback angle of quarter-chord line, deg	35	
Taper ratio	0.61	
Airfoil section (streamwise).	NACA 64 ₁ A012	
Area, sq ft (m ²).	5.135 (0.4774)	
Mean aerodynamic chord, ft (m)	2.073 (0.6318)	
Span, ft (m)	2.53 (0.771)	
Elastic-axis location, fraction of vertical-tail chord (streamwise).	0.39	0.40
Length along elastic axis, ft (m)	2.78 (0.847)	2.74 (0.835)
Rudder:		
Spanwise location, fraction of fin span, at -		
Root	0.0	
Tip	0.84	
Chordwise location, fraction of vertical-tail chord (streamwise), at -		
Leading edge	0.716	
Trailing edge	1.00	
Hinge axis, fraction of vertical-tail chord (streamwise)	0.77	0.75
Exposed area, fraction of vertical-tail area	0.20	0.22

^aValues for model of reference 10 are given only when different from those for the present model.

TABLE II.- SUMMARY OF MODEL CONFIGURATIONS USED IN FLUTTER TESTS

Configuration (a)	f_{θ} , cps	Fin spar	Rudder		Elevators				Bullet fairing (see fig. 9)	Vortex-generator location, percent streamwise chord		Comments
			f_r , cps	ξ	Left		Right			Fin	Stabilizers	
					f_e , cps	ξ	f_e , cps	ξ				
Tests in air												
W1-1	65	1	Locked		Locked		Locked		1 (original)	None		Weakened-fin-spar configuration. Added vortex generators to fin. Lost empennage during flutter.
W1-2	65	1	Locked		Locked		Locked		1 (original)	35	None	
Tests in freon												
D1-1	66	2	39.3	0.102	38.6	0.031	38.5	0.032	1	35	None	Nominal design configuration. All rebuilt to be same as configuration W1-1, except fin spar.
D1-2	66	2	6.25	----	10.7	.088	12.5	.15	1	35	None	
D1-3	66	2	6.25	----	10.7	.088	12.5	.15	2	35	None	Modified bullet fairing shape.
D1-4	66	2	21.0	.08	21.6	.047	22.8	.039	2	35	35	Configuration with intermediate rotational stiffness of control surfaces.
D2-1	51	2	37.5	.101	38.5	.068	39.3	.069	2	35	35	Reduced stabilizer pitch-spring stiffness.
D3-1	32	2	37.5	.101	38.5	.068	39.3	.069	2	35	35	
D1-5	65	2	38.0	.10	37.5	.03	40.0	.07	1	35	35	Nominal design configuration with fences on bullet fairing.

^aD designates design configuration; W indicates configuration with weakened fin spar. The first number designates pitch spring used; last number indicates variations in control rotational stiffness, bullet fairing shape, or vortex-generator configuration.

TABLE III.- MASS PROPERTIES OF MODEL CONFIGURATIONS

(a) Major model components

Total model (design configuration D1-1):

Mass, slugs (kg)	9.04 (132)
Center of gravity, in. (cm)	FS 101.9 (258.8)

Fuselage mass, slugs (kg) 2.96 (43.2)

Wing and pylon-nacelle:

Wing mass (full span), slugs (kg)	4.085 (59.62)
Pylon-nacelle mass (both sides), slugs (kg)	1.652 (24.11)
Inertia in roll about fuselage center line, slug-ft ² (kg-m ²)	50.15 (67.99)

Empennage (design configuration D1-1):

Total empennage mass, $m_{e,o}$, slugs (kg)	0.3401 (4.963)
Vertical-tail mass, $m_{v,o}$, slugs (kg)	0.1680 (2.452)

Horizontal tail^a:

Mass, $m_{h,o}$, slugs (kg)	0.1721 (2.512)
Center of gravity	FS 204.3 (518.9)
$I_{\theta,o}$, slug-ft ² (kg-m ²)	0.04802 (0.06511)
$I_{\psi,o}$, slug-ft ² (kg-m ²)	0.3180 (0.4312)
$I_{\phi,o}$, slug-ft ² (kg-m ²)	0.2920 (0.3959)

Configurations	Horizontal tail ^a						$\frac{m_v}{m_{v,o}}$	$\frac{m_e}{m_{e,o}}$
	Center of gravity in. (cm)	$\frac{I_{\theta}}{I_{\theta,o}}$	$\frac{I_{\psi}}{I_{\psi,o}}$	$\frac{I_{\phi}}{I_{\phi,o}}$	$\frac{m_h}{m_{h,o}}$			
W1-1, W1-2	} FS 204.3 (518.9)	1.06	1.06	1.06	1.06	0.99	1.02	
D1-1, D1-2		1.00	1.00	1.00	1.00	1.00	1.00	
D1-3, D1-4, D2-1, D3-1		1.04	1.00	1.00	1.01	1.00	1.01	
D1-5		1.06	1.00	1.00	1.05	1.00	1.02	

^aIncludes stabilizer, elevators, and bullet fairing.

TABLE III.- MASS PROPERTIES OF MODEL CONFIGURATIONS - Concluded

(b) Empennage components

Stabilizer without elevator														
Section ^b	Section limits, η_{ea}		Configuration W						Configuration D					
			Mass		S_{ea}		I_{ea}		Mass		S_{ea}		I_{ea}	
			slugs	kg	slug-ft	kg-m	slug-ft ²	kg-m ²	slugs	kg	slug-ft	kg-m	slug-ft ²	kg-m ²
0	0	to 0.066	0.0140	0.204	0.491×10^{-3}	0.00218	0.672×10^{-3}	0.000911	0.0140	0.204	0.491×10^{-3}	0.002184	0.672×10^{-3}	0.000911
1	.066	to .222	.0135	.197	-.648	-.00288	.785	.001064	.0132	.193	-.446	-.001984	.832	.001128
2	.222	to .379	.0112	.163	.077	.00034	.616	.000835	.0106	.155	.127	.000565	.631	.000856
3	.379	to .535	.0087	.127	-.111	-.00049	.336	.000456	.0081	.118	-.079	-.000351	.346	.000469
4	.535	to .692	.0075	.110	-.121	-.00054	.251	.000340	.0068	.099	-.086	-.000382	.237	.000321
5	.692	to .848	.0061	.089	-.131	-.00058	.148	.000201	.0053	.077	-.131	-.000583	.140	.000190
6	.848	to 1.000	.0052	.076	-.032	-.00014	.082	.000111	.0048	.070	.078	.000347	.090	.000122
Total	0	to 1.000	0.0662	0.966	-0.475×10^{-3}	-0.00211	2.890×10^{-3}	0.003918	0.0628	0.916	-0.046×10^{-3}	-0.000204	2.948×10^{-3}	0.003997

Control surfaces													
Surface	Mass balance, percent	Configuration W						Configuration D					
		Mass		S_{hl}		I_{hl}		Mass		S_{hl}		I_{hl}	
		slugs	kg	slug-ft	kg-m	slug-ft ²	kg-m ²	slugs	kg	slug-ft	kg-m	slug-ft ²	kg-m ²
Elevator	100	0.0164	0.239	0.000091	0.00041	0.000113	0.000153	0.0156	0.228	0.000132	0.000587	0.000124	0.000168
Rudder	0	.0128	.187	.001330	.00592	.000422	.000572	.0138	.201	.001491	.006632	.000442	.000599

Fin without rudder														
Section ^c	Section limits, η_{ea}		Configuration W						Configuration D					
			Mass		S_{ea}		I_{ea}		Mass		S_{ea}		I_{ea}	
			slugs	kg	slug-ft	kg-m	slug-ft ²	kg-m ²	slugs	kg	slug-ft	kg-m	slug-ft ²	kg-m ²
1	0	to 0.305	0.0411	0.600	-7.19×10^{-3}	-0.0320	7.87×10^{-3}	0.01067	0.0457	0.667	-8.65×10^{-3}	-0.0385	8.92×10^{-3}	0.01209
2	.305	to .506	.0245	.358	0	0	3.24	.00439	.0232	.338	.83	.0037	2.75	.00373
3	.506	to .712	.0232	.338	.66	.0029	2.47	.00335	.0224	.327	.66	.0029	2.17	.00294
4	.712	to 1.000	.0637	.930	-2.09	-.0093	9.18	.01245	.0629	.918	-2.16	-.0096	7.54	.01022
Total	0	to 1.000	0.1525	2.226	-8.62×10^{-3}	-0.0384	22.76×10^{-3}	0.03086	0.1542	2.250	-9.32×10^{-3}	-0.0415	21.38×10^{-3}	0.02899

Bullet fairing								
Configuration	Mass		Center of gravity		I_{ψ}		I_{θ}	
	slugs	kg	in.	cm	slug-ft ²	kg-m ²	slug-ft ²	kg-m ²
1 (Original)	0.0172	0.251	201.0	510.5	9.81×10^{-3}	0.0133	10.0×10^{-3}	0.0136
d ₁	.0153	.223	200.7	509.8	8.68	.0118	9.04	.0122
2	.0180	.263	201.6	512.1	10.7	.0145	10.7	.0145
d,e ₁	.0222	.324	201.0	510.5	12.1	.0164	11.4	.0154

^bSections outlined in figure 1(b).

^cSections outlined in figure 1(c).

^dBullet fairing rebuilt to original shape.

^eIncludes fences.

TABLE IV.- STIFFNESSES OF STABILIZER PITCH SPRINGS AND FIN-STABILIZER JOINTS

[Sign convention of deflections and applied moments referenced to stabilizer chord plane:
Positive roll, right stabilizer tip downward; positive yaw, right stabilizer tip rearward]

(a) Pitch spring stiffness

Spring	Pitch stiffness	
	in-lb/radian	m-N/radian
^a 1 (Design)	100.2×10^3	11 320
2	58.2	6 580
3	23.9	2 700

^aRebuilt pitch spring 1 had same stiffness as original spring 1.

(b) Fin-stabilizer joint stiffness^a

Fin spar	Yaw due to yawing moment		Yaw due to rolling moment		Roll due to yawing moment		Roll due to rolling moment	
	in-lb/radian	m-N/radian	in-lb/radian	m-N/radian	in-lb/radian	m-N/radian	in-lb/radian	m-N/radian
1	61.2×10^3	6 910	-134×10^3	-15 100	-147×10^3	-16 600	50.2×10^3	5 670
2	195	22 000	-351	-39 600	-351	-39 600	234	26 400

^aStiffnesses were measured between station on fin elastic axis at WL 58.46 in. (148.49 cm) and the point on underside of stabilizer spar at elastic axis where the bracket arm is attached.

TABLE V.- MEASURED NATURAL FREQUENCIES OF MODEL

Vibration mode	Frequency, cps, of configuration -		
	D1 (a)	W1 (a)	W1 (b)
Symmetric			
Model pitch	0.89	1.10	
Model vertical translation	1.50	1.15	
Model fore-and-aft translation	2.10	2.20	
Wing bending	9.6	9.32	
Fuselage vertical bending	12.2	11.98	11.88
Engine pitch	16.1	15.9	
Stabilizer first bending	21.0	20.7	21.9
Fin fore-and-aft bending	23.0	23.1	
	27.0	26.9	
	29.7		48.3
Stabilizer bending	60.0		
Stabilizer pitch	79.3	80.0	71.5
Stabilizer first torsion	89.9	92.0	89.0
Stabilizer second torsion	111.3		
Antisymmetric			
Model yaw	0.35		
Model roll	.92	1.0	
Model lateral translation	1.80	1.90	
Fin bending, aft-fuselage torsion	6.30	5.15	5.05
Fin torsion		9.0	8.69
Stabilizer roll	10.40	10.8	
Stabilizer yaw	13.30		14.52
	15.0	15.3	
Fin bending	18.8	17.0	
	22.0	21.6	
Stabilizer bending, fin bending	30.0	29.3	
		39.5	
	53.2	51.5	52.0
	64.0	59.9	
	76.8		74.0
Stabilizer torsion	88.8	92.0	80.0
	103.0		
	127.5		

^aConfiguration mounted in tunnel with control surfaces locked.

^bEmpennage cantilevered at fuselage station 158.8 in. (403.4 cm) with control surfaces locked.

TABLE VI.- COMPILATION OF TEST RESULTS

(a) Weakened-fin-spar configurations tested in air

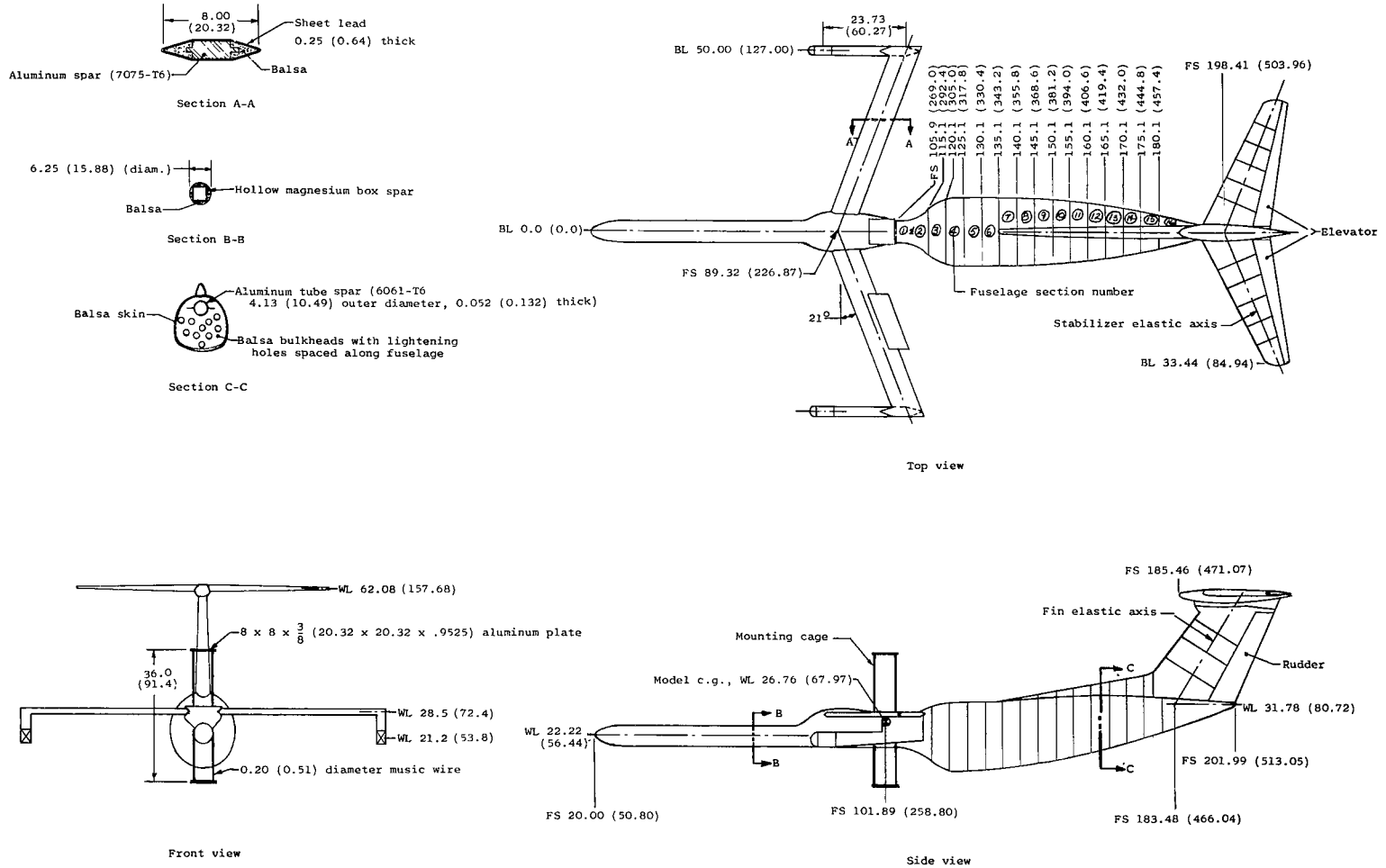
Configuration	Model behavior ^a	M	q		ρ		V		α _t , deg	N _{Re}		μ	f, cps
			lb/sq ft	kN/m ²	slug/ft ³	kg/m ³	ft/sec	m/s		ft ⁻¹	m ⁻¹		
W1-1	NF	0.904	54.1	2.59	0.000114	0.059	973.9	296.8	0.3	0.31 × 10 ⁶	1.02 × 10 ⁶	298.5	---
	NF	.904	86.0	4.12	.000179	.092	980.8	298.9	.2	.49	1.61	190.1	---
W1-2	NF	.723	86.6	4.15	.000270	.139	801.6	244.3	-.2	.58	1.90	126.0	---
	NF	.802	101.3	4.85	.000260	.134	882.6	269.0	-.5	.63	2.07	130.9	---
	NF	.899	119.0	5.70	.000248	.128	980.4	298.8	0	.67	2.20	137.2	---
	NF	.596	77.7	3.72	.000344	.177	672.2	204.9	-.2	.61	2.00	98.9	---
	F	.698	100.6	4.82	.000331	.171	779.1	237.5	-.3	.69	2.26	102.8	7.25

^aModel behavior code: F - antisymmetric flutter; NF - no flutter.

TABLE VI.- COMPILATION OF TEST RESULTS - Concluded

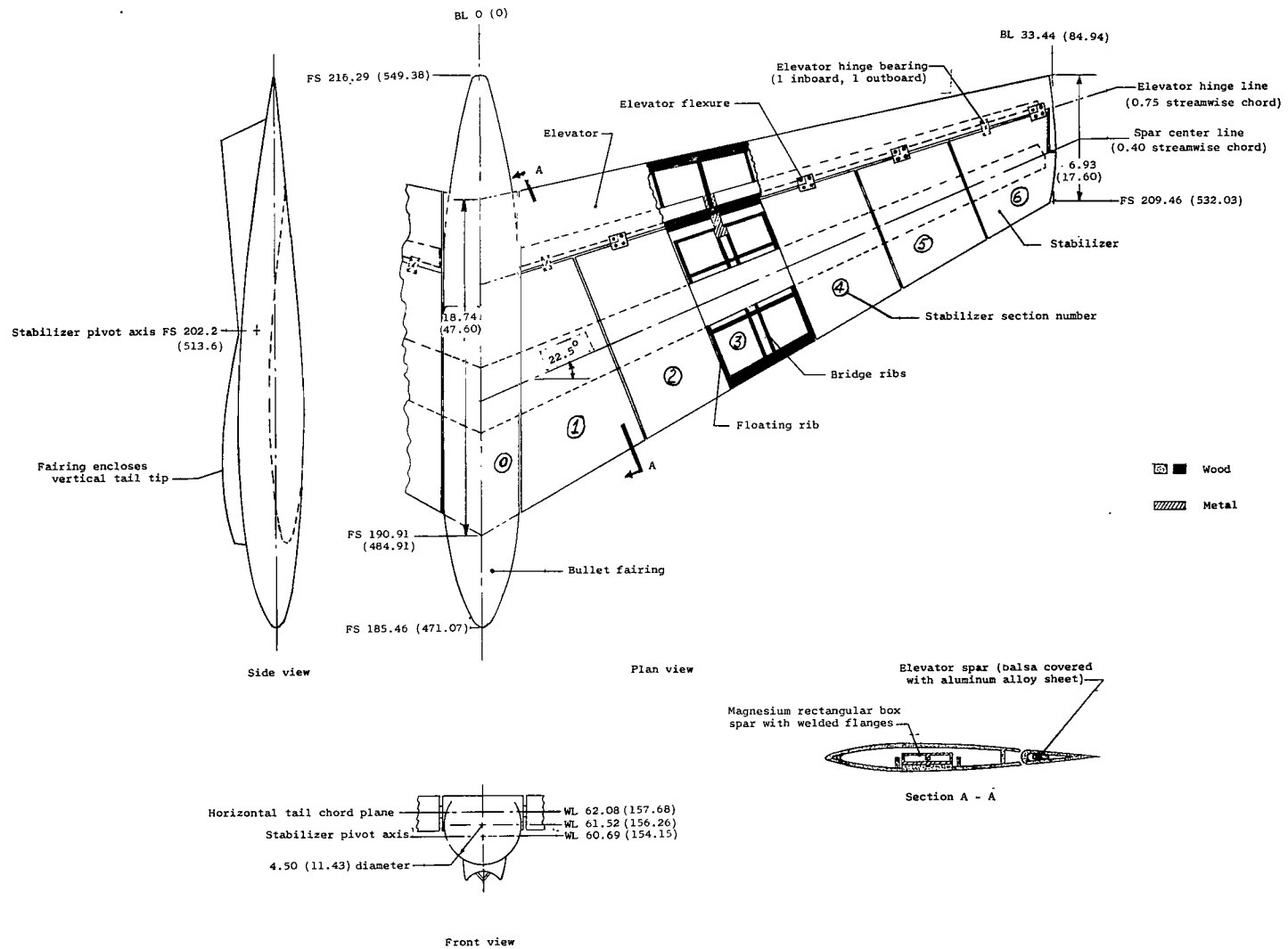
(b) Design configurations tested in freon; all data represent no-flutter conditions

M	q		slug/ft ³	ρ kg/m ³	α _t , deg	NRe		μ
	lb/sq ft	kN/m ²				ft-1	m-1	
Configuration D1-1								
0.86	34.0	1.63	-----	-----	-----	-----	-----	---
.895	46.5	2.23	0.000460	0.237	0.1	0.78 × 10 ⁶	2.56 × 10 ⁶	69.8
.903	58.7	2.81	.000654	.291	.2	.96	3.15	56.9
.900	65.7	3.14	.000639	.329	.2	1.09	3.58	50.3
.904	82.2	3.94	.000790	.407	.7	1.35	4.43	40.6
.900	100.0	4.79	.000968	.499	.4	1.65	5.41	33.2
.904	136.8	6.55	.001292	.666	.4	2.20	7.22	24.9
.745	142.2	6.81	.001948	1.004	.3	2.73	8.96	16.5
.674	144.0	6.89	.002409	1.242	.5	3.05	10.01	13.3
.636	145.2	6.95	.002729	1.406	.3	3.25	10.66	11.8
Configuration D1-2								
0.636	144.8	6.93	0.002726	1.405	-----	3.26 × 10 ⁶	10.70 × 10 ⁶	11.8
.718	141.3	6.76	.002099	1.082	-----	2.83	9.28	15.3
.811	142.5	6.82	.001665	.858	-----	2.54	8.33	19.3
.900	137.1	6.56	.001311	.676	-----	2.23	7.32	24.5
Configuration D1-3								
0.896	134.4	6.44	0.001324	0.682	-----	2.25 × 10 ⁶	7.38 × 10 ⁶	24.6
.890	81.4	3.90	.000814	.420	-----	1.38	4.53	40.1
.893	45.9	2.20	.000452	.233	-----	.76	2.49	72.2
.868	36.8	1.76	.000382	.197	-----	.63	2.07	85.4
Configuration D1-4								
0.860	35.9	1.72	0.000378	0.195	0.1	0.61 × 10 ⁶	2.00 × 10 ⁶	86.3
.907	45.9	2.20	.000432	.223	.9	.74	2.43	75.5
.902	79.8	3.82	.000769	.396	.7	1.31	4.30	42.4
.904	137.2	6.57	.001323	.682	.6	2.27	7.45	24.6
.787	142.9	6.84	.001806	.931	.2	2.69	8.82	18.1
.708	144.6	6.92	.002247	1.158	.4	3.00	9.84	14.5
.625	145.0	6.94	.002882	1.485	.2	3.40	11.15	11.3
Configuration D2-1								
0.909	39.0	1.87	0.000366	0.189	1.4	0.63 × 10 ⁶	2.07 × 10 ⁶	89.1
.904	48.1	2.30	.000456	0.235	.3	.78	2.56	71.5
.904	80.4	3.85	.000771	0.397	.5	1.32	4.33	42.3
.897	135.6	6.49	.001334	0.688	.5	2.27	7.45	24.5
.781	143.2	6.86	.001833	0.945	0.2 to 1.2	2.71	8.89	17.8
.698	146.2	7.00	.002331	1.201	0.4 to 1.4	3.07	10.07	14.0
.640	146.2	7.00	.002764	1.424	0.3 to 1.2	3.33	10.92	11.8
Configuration D3-1								
0.874	36.0	1.72	0.000366	0.189	-0.2	0.60 × 10 ⁶	1.97 × 10 ⁶	89.1
.914	45.7	2.19	.000426	.220	1.1	.73	2.39	76.6
.907	76.5	3.66	.000732	.377	1.0	1.26	4.13	44.6
.905	137.5	6.58	.001321	.681	.7	2.26	7.41	24.7
.787	143.0	6.85	.001797	.926	.4	2.67	8.76	18.2
.707	142.6	6.83	.002210	1.139	.6	2.95	9.68	14.8
.617	147.5	7.06	.002986	1.539	.4	3.46	11.35	10.9
Configuration D1-5								
0.865	36.0	1.72	0.000356	0.183	-----	0.57 × 10 ⁶	1.87 × 10 ⁶	93.8
1.085	57.8	2.77	.000366	.189	-----	.74	2.43	91.2
1.083	87.4	4.18	.000568	.293	-----	1.15	3.77	58.8
1.077	131.2	6.28	.000868	.447	2.8	1.76	5.77	38.5
.931	166.7	7.98	.001473	.759	1.5	2.58	8.46	22.7
.826	154.6	7.40	.001713	.883	.7	2.65	8.73	19.5
.746	166.6	7.98	.002252	1.161	.9	3.14	10.30	14.8
.704	177.6	8.50	.002684	1.383	1.1	3.54	11.61	12.4



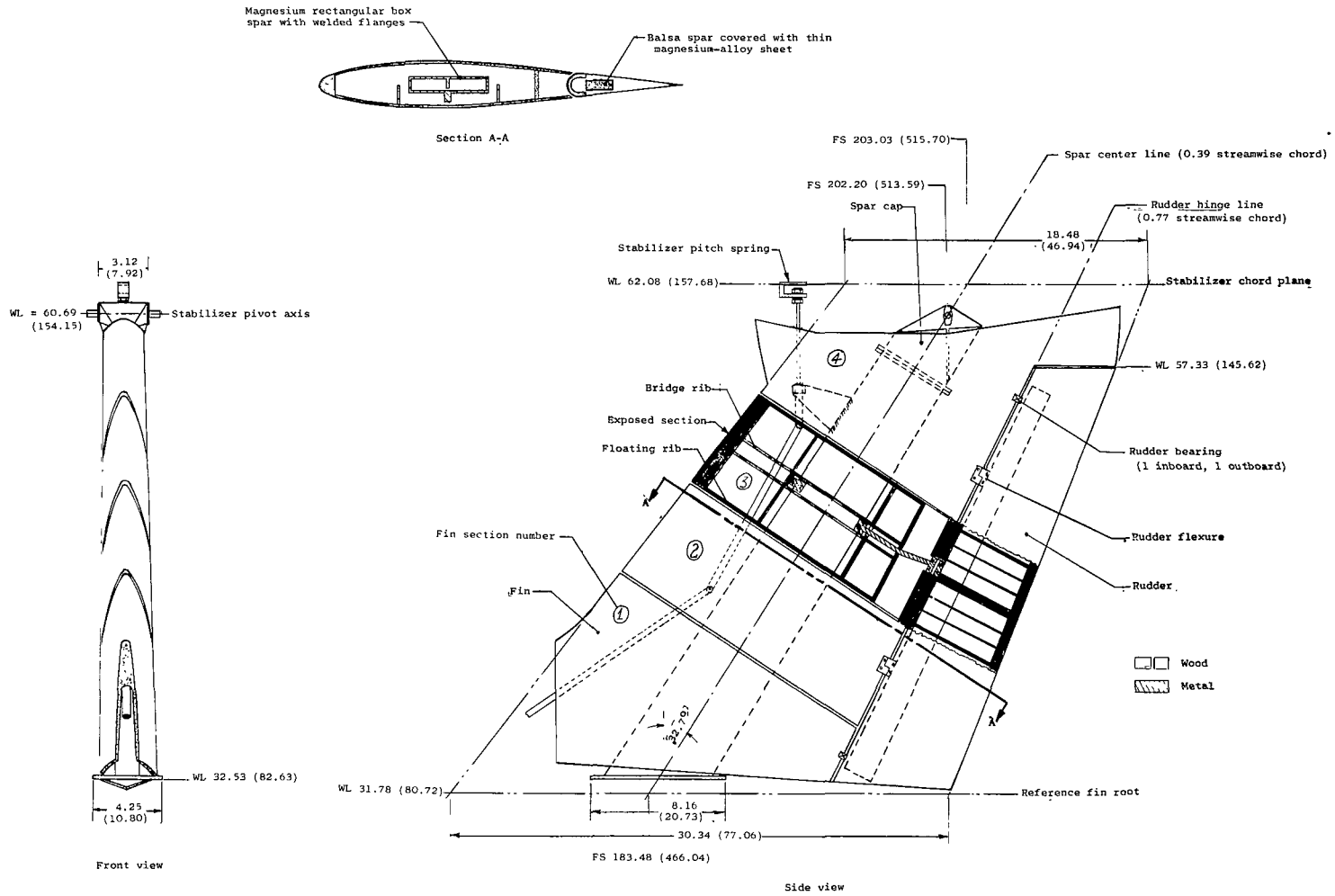
(a) Complete model.

Figure 1.- Sketches of model. All dimensions are in inches (centimeters) except as noted otherwise.



(b) Horizontal tail.

Figure 1.- Continued.



(c) Vertical tail.

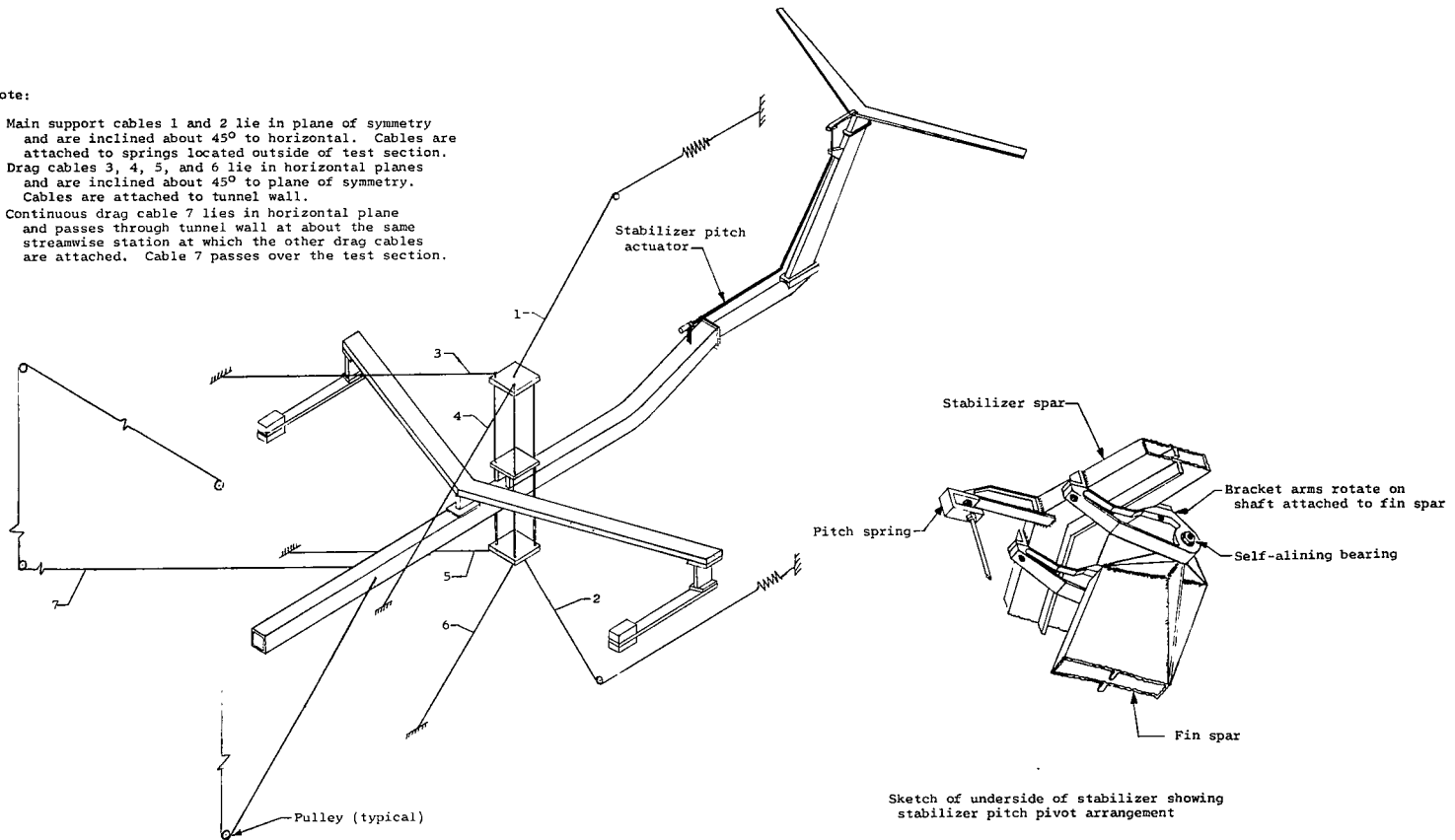
Figure 1.- Continued.

Note:

Main support cables 1 and 2 lie in plane of symmetry and are inclined about 45° to horizontal. Cables are attached to springs located outside of test section.

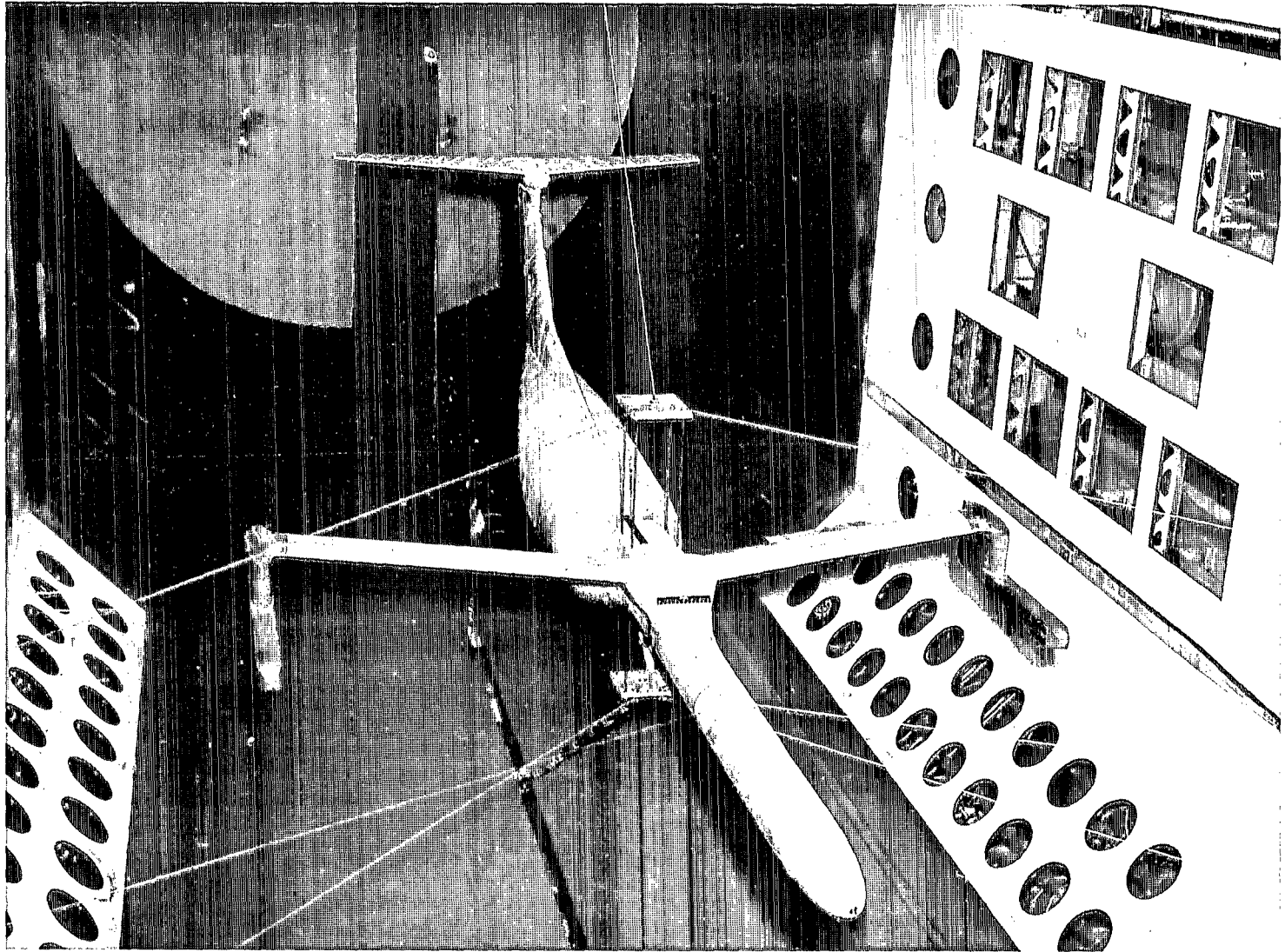
Drag cables 3, 4, 5, and 6 lie in horizontal planes and are inclined about 45° to plane of symmetry. Cables are attached to tunnel wall.

Continuous drag cable 7 lies in horizontal plane and passes through tunnel wall at about the same streamwise station at which the other drag cables are attached. Cable 7 passes over the test section.



(d) Sketch showing main structural members of model and mount system.

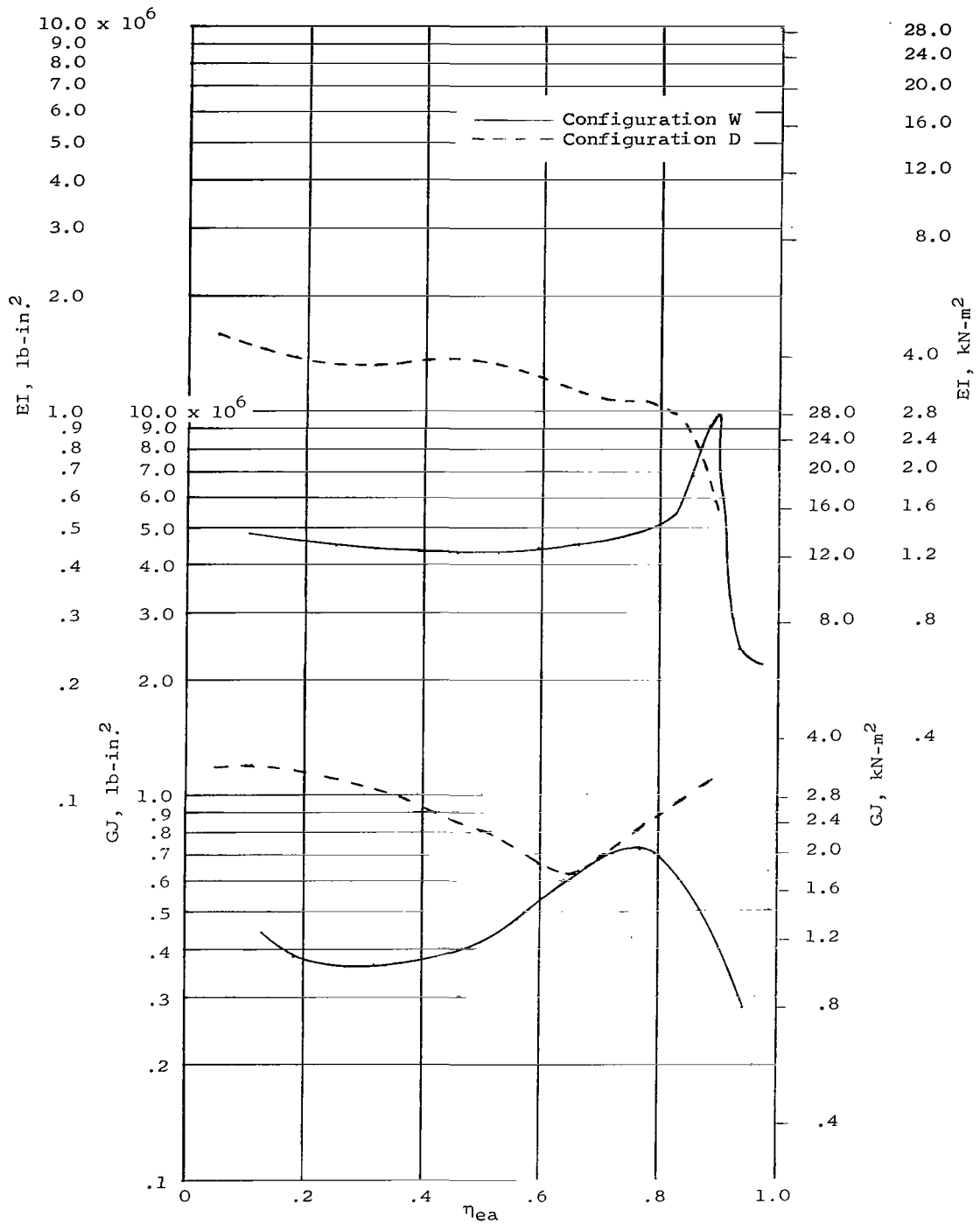
Figure 1.- Concluded.



(a) Model suspended in tunnel.

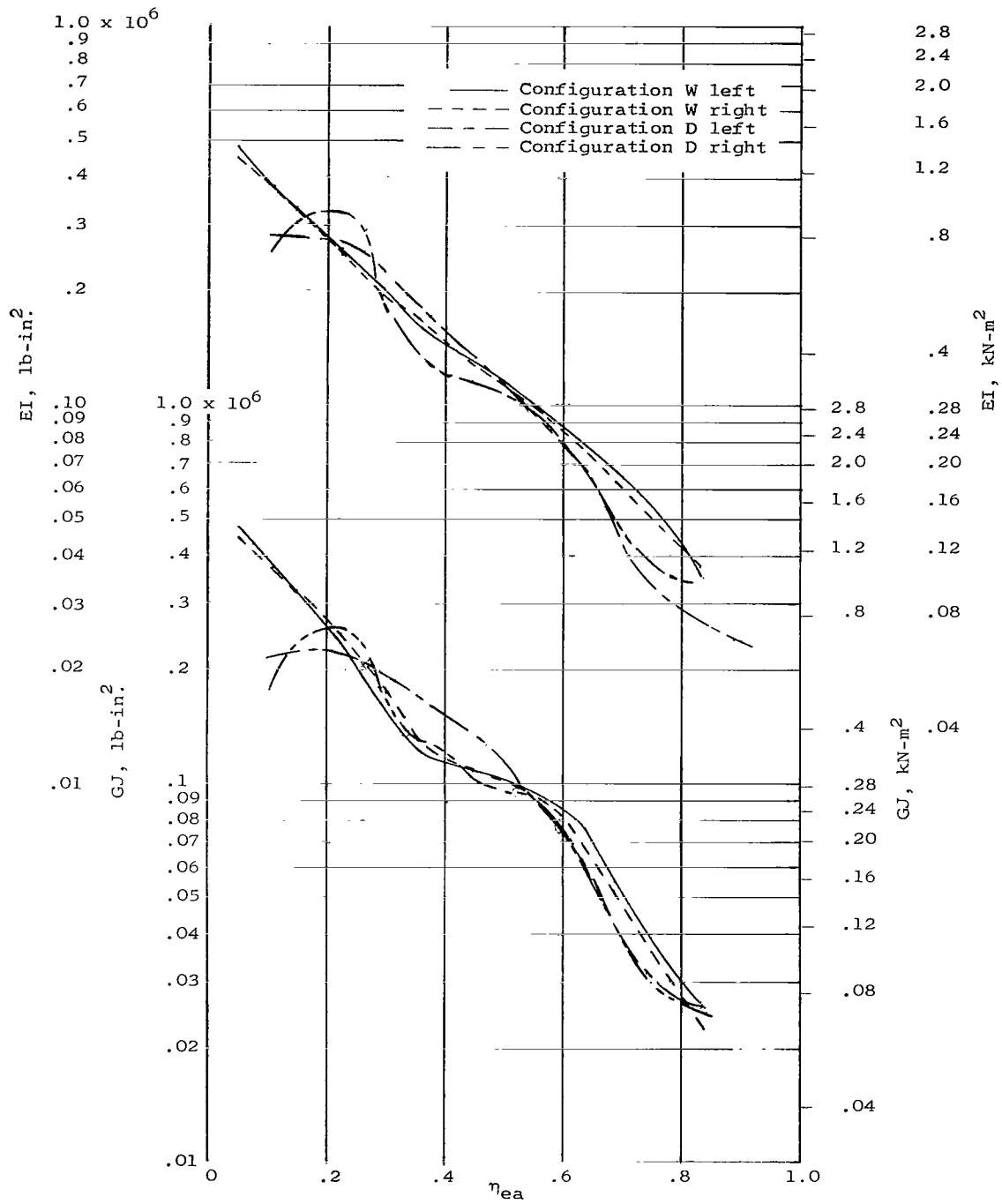
Figure 2.- Photographs of model.

L-62-6734



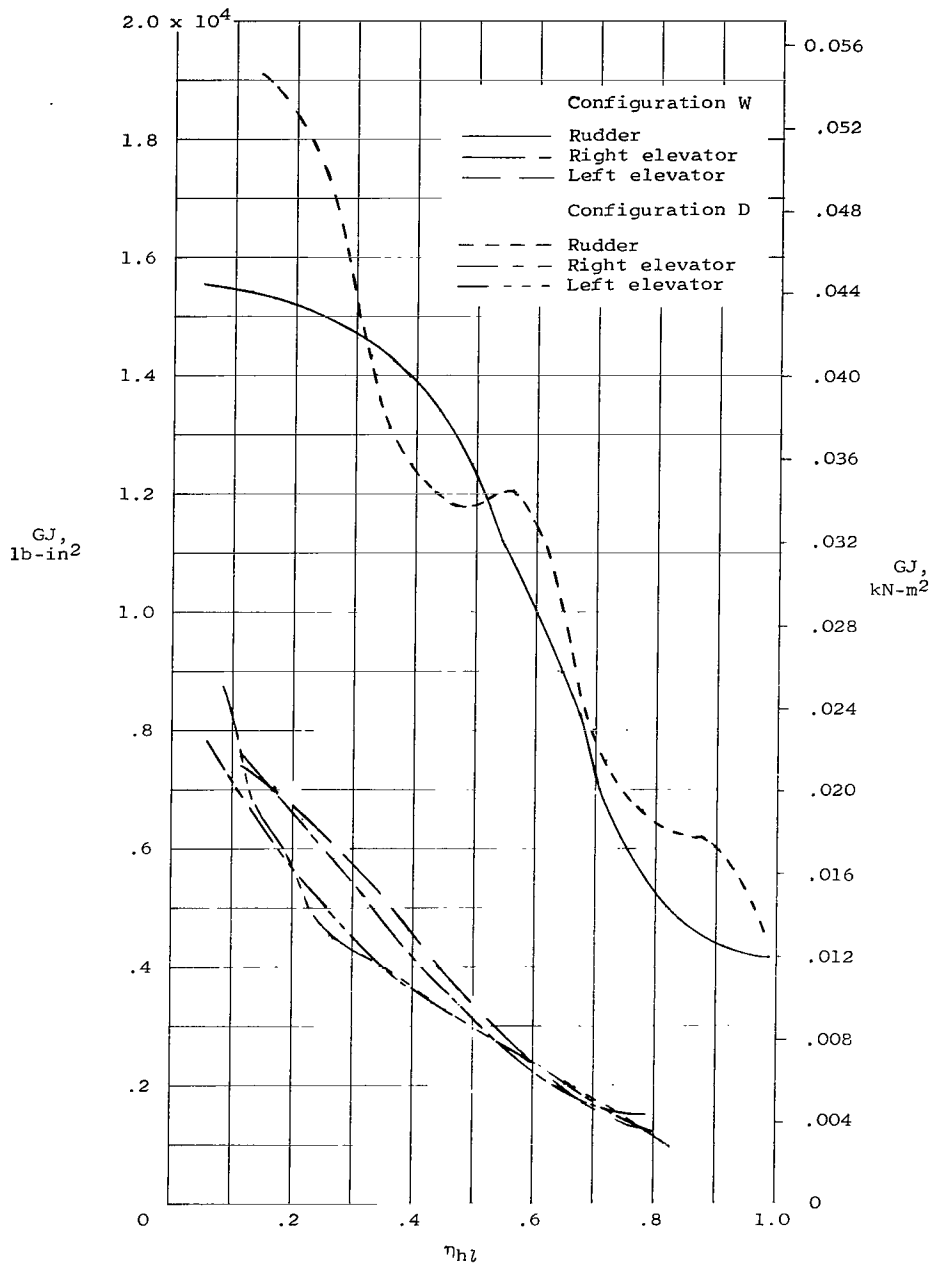
(a) Fin spars.

Figure 3.- Measured distributions of bending and torsional stiffness of model components.



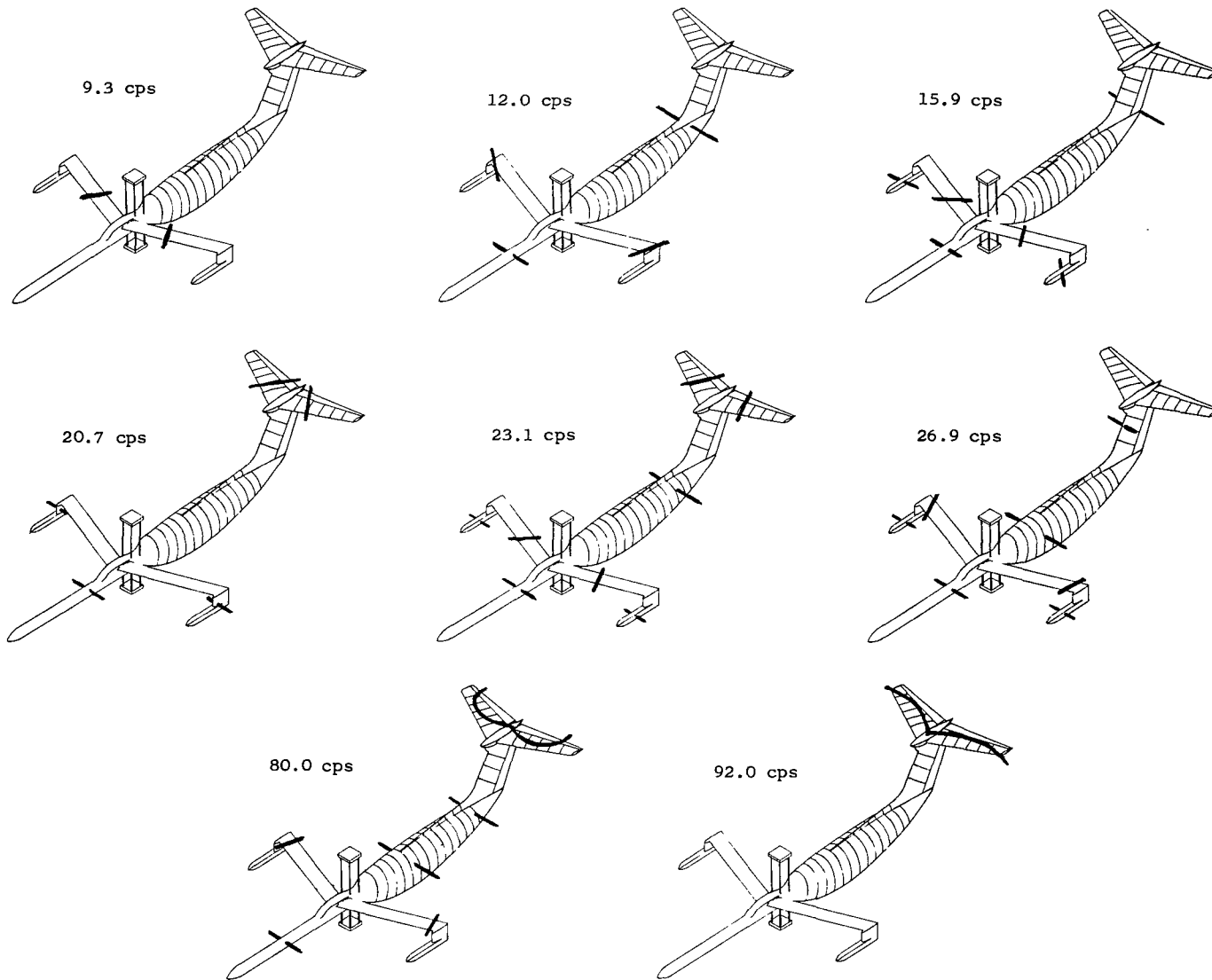
(b) Stabilizer spars.

Figure 3.- Continued.



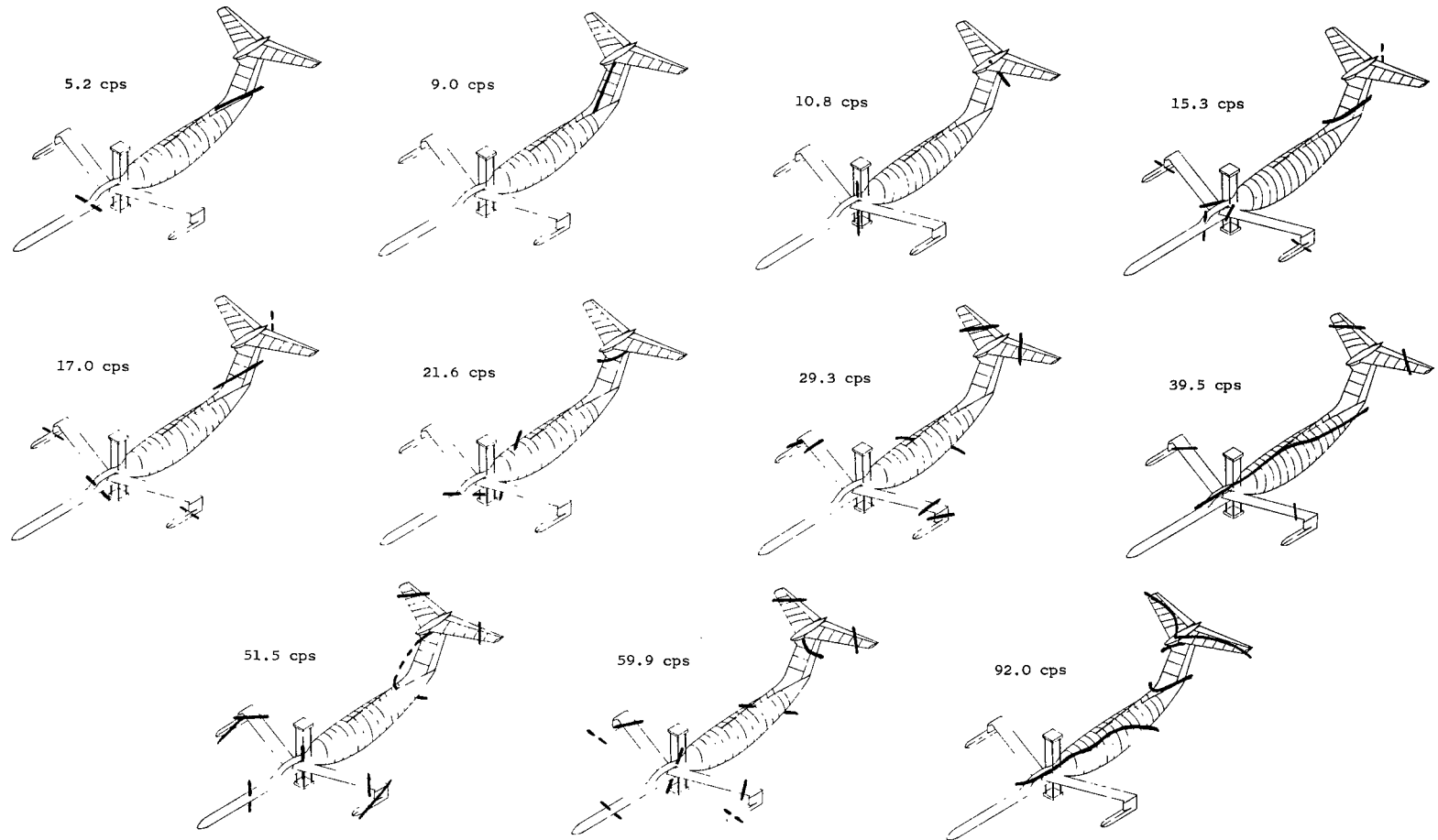
(c) Rudders and elevators.

Figure 3.- Concluded.



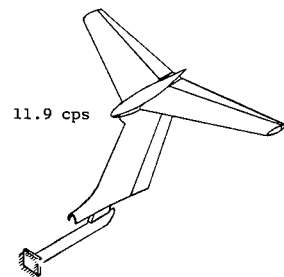
(a) Symmetric modes.

Figure 4.- Measured node lines associated with natural vibration frequencies for configuration W1 with control surfaces locked.

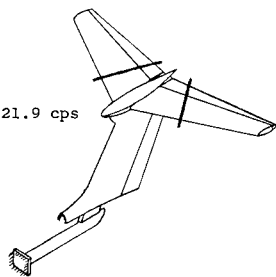


(b) Antisymmetric modes.

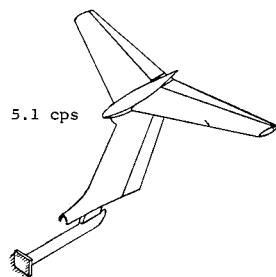
Figure 4.- Concluded.



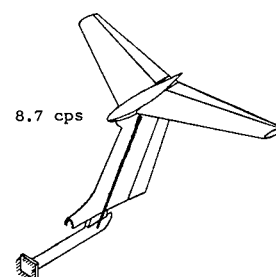
11.9 cps



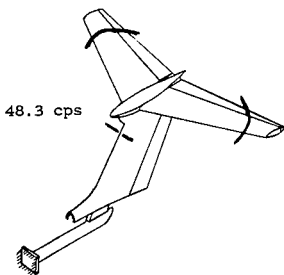
21.9 cps



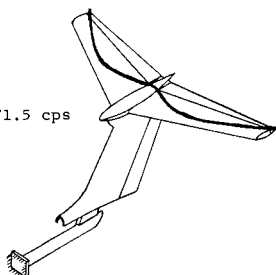
5.1 cps



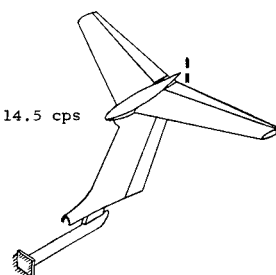
8.7 cps



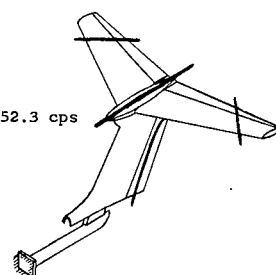
48.3 cps



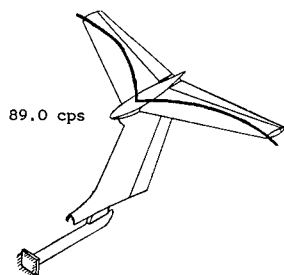
71.5 cps



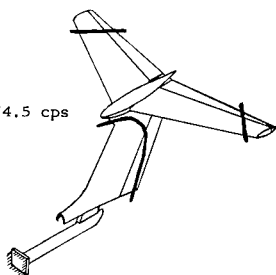
14.5 cps



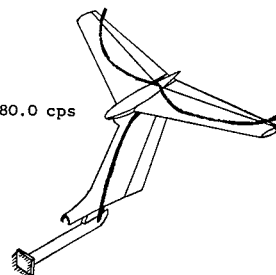
52.3 cps



89.0 cps



74.5 cps

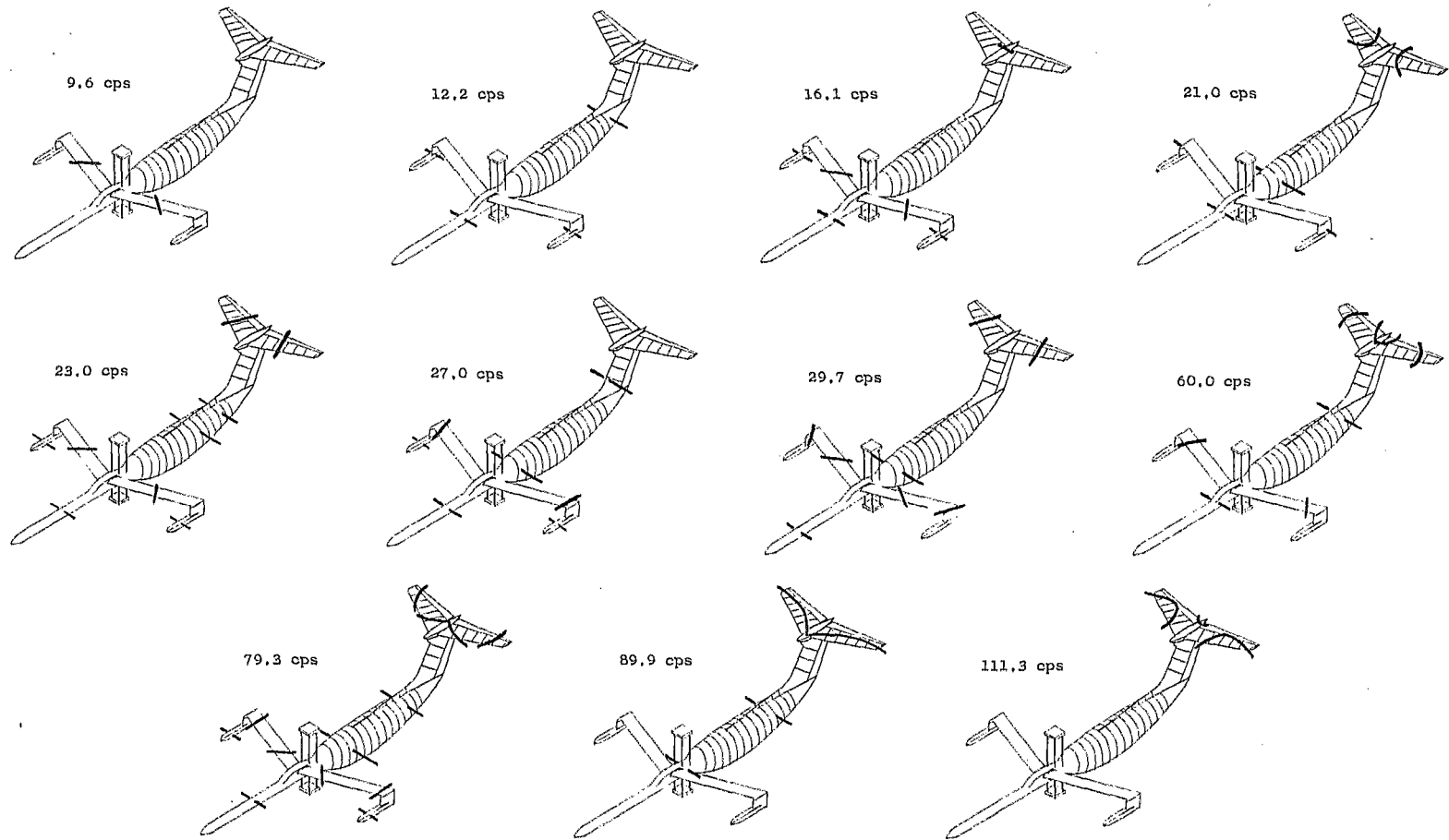


80.0 cps

(a) Symmetric modes.

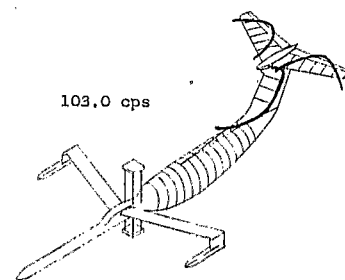
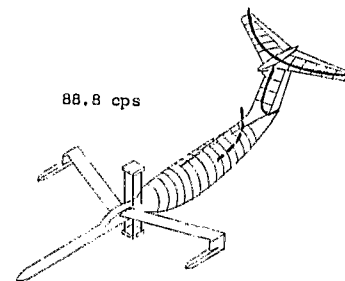
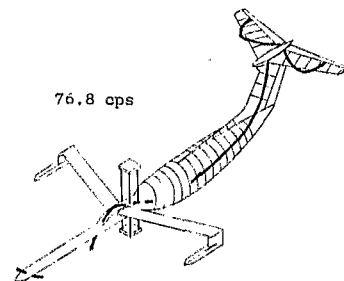
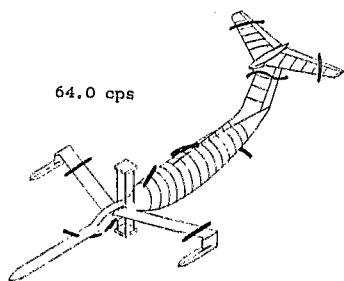
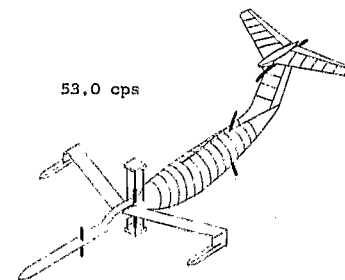
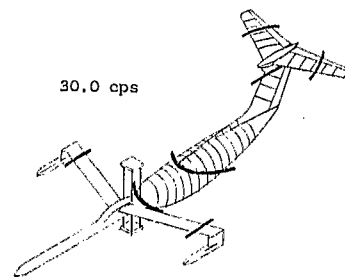
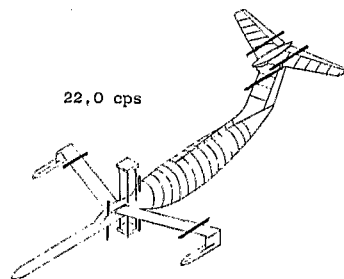
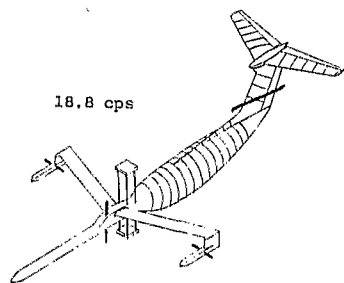
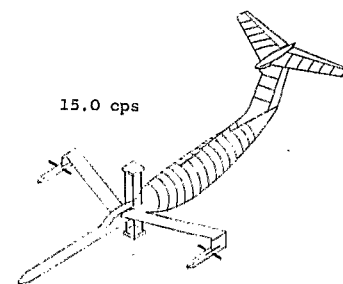
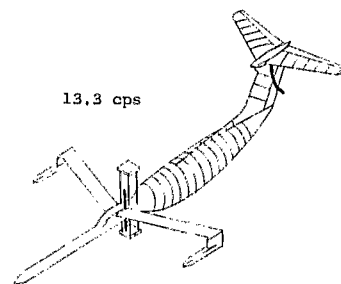
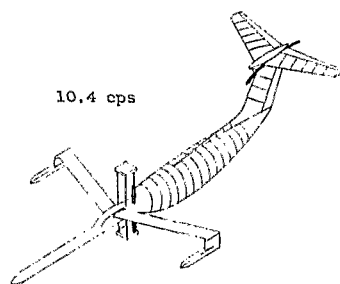
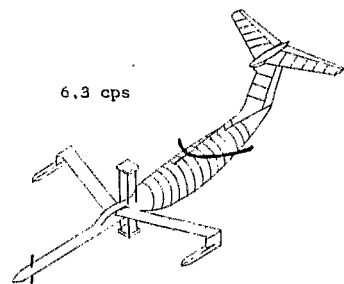
(b) Antisymmetric modes.

Figure 5.- Measured node lines associated with natural vibration frequencies for configuration W1 cantilevered at fuselage station 158.8 inches (403.4 cm) with control surfaces locked.



(a) Symmetric modes.

Figure 6.- Measured node lines associated with natural vibration frequencies for configuration D1 with control surfaces locked.



(b) Antisymmetric modes.

Figure 6.- Concluded.

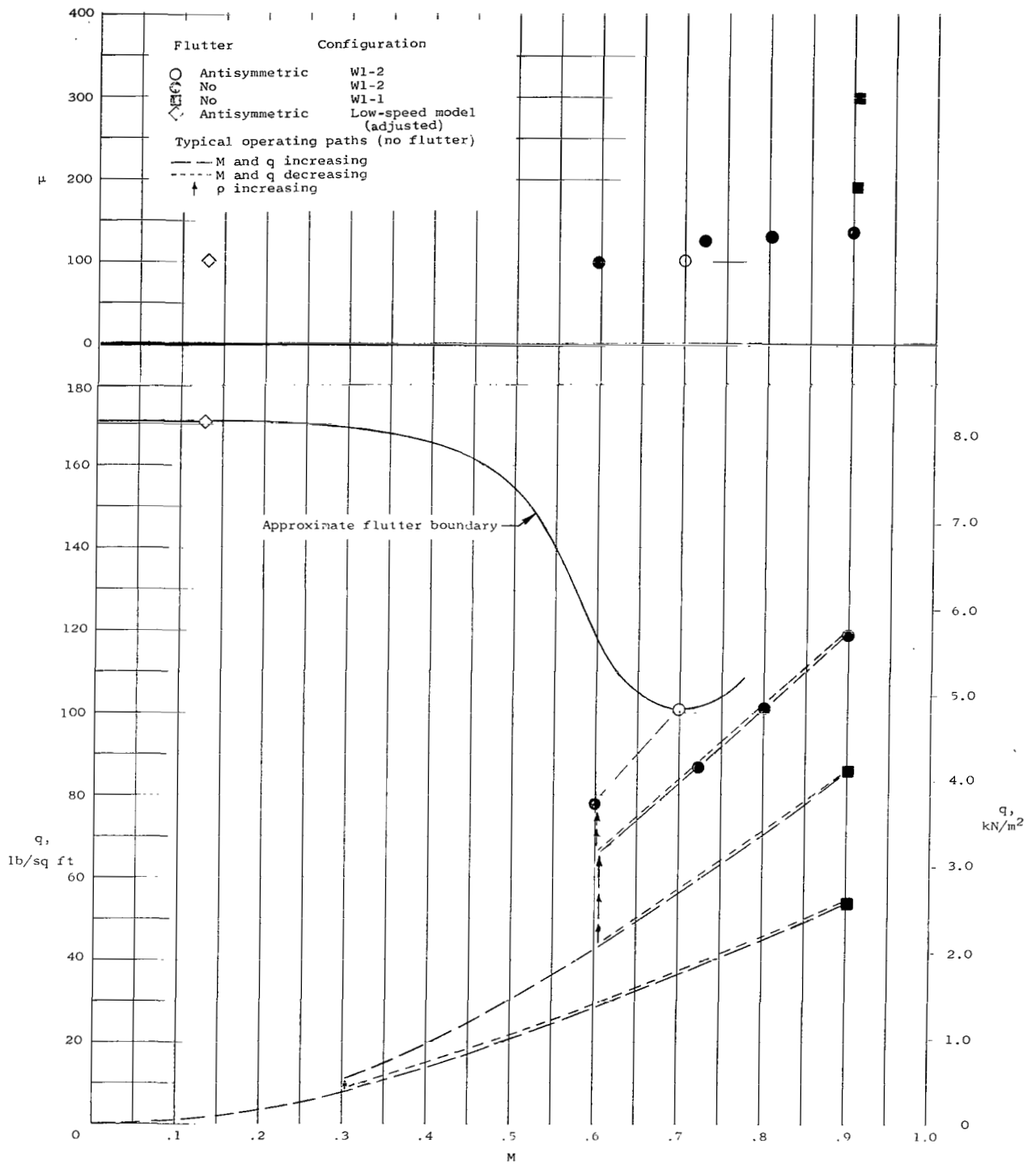


Figure 7.- Dynamic pressures, mass ratios, and Mach numbers covered for weakened-fin configurations in air.

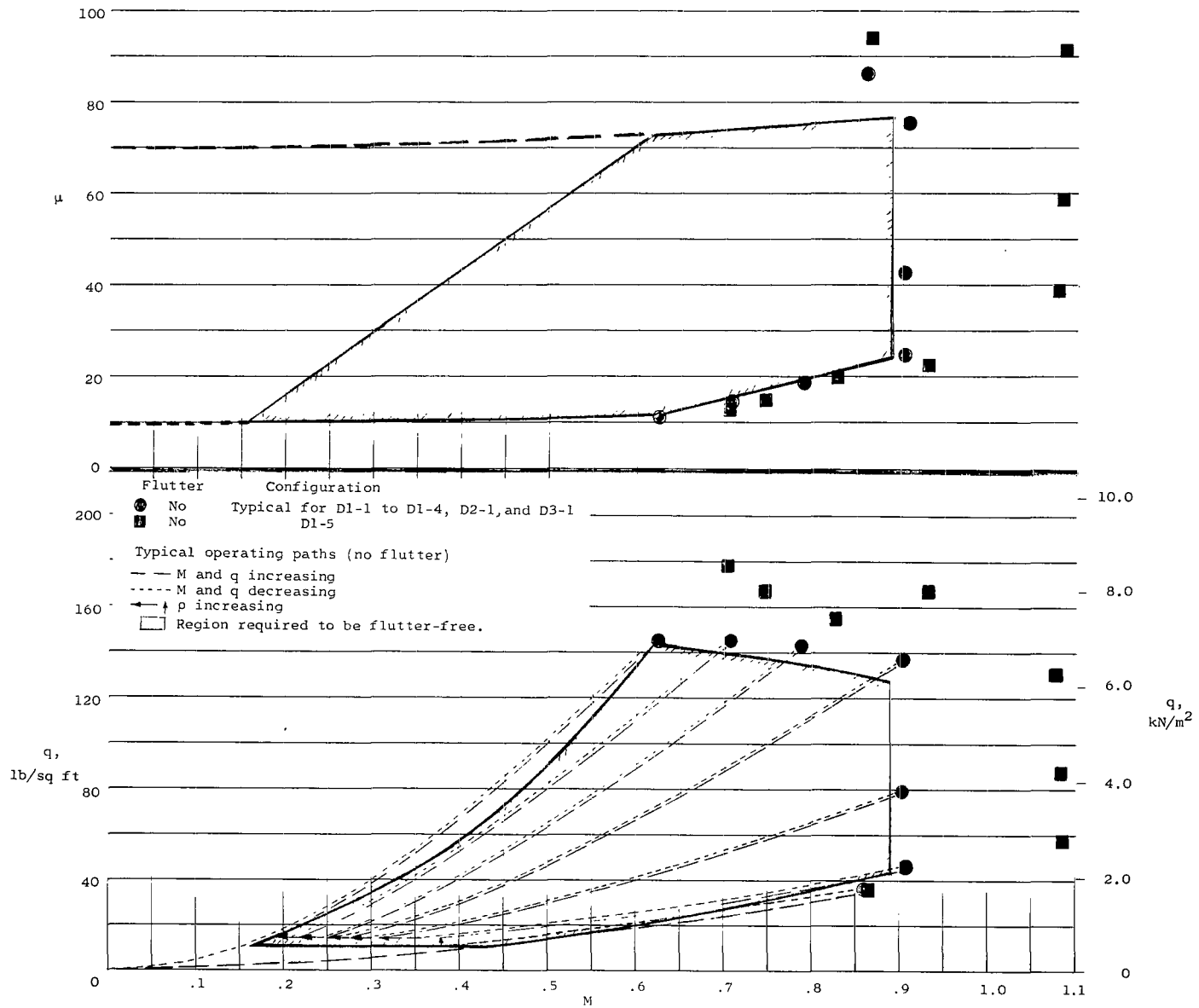
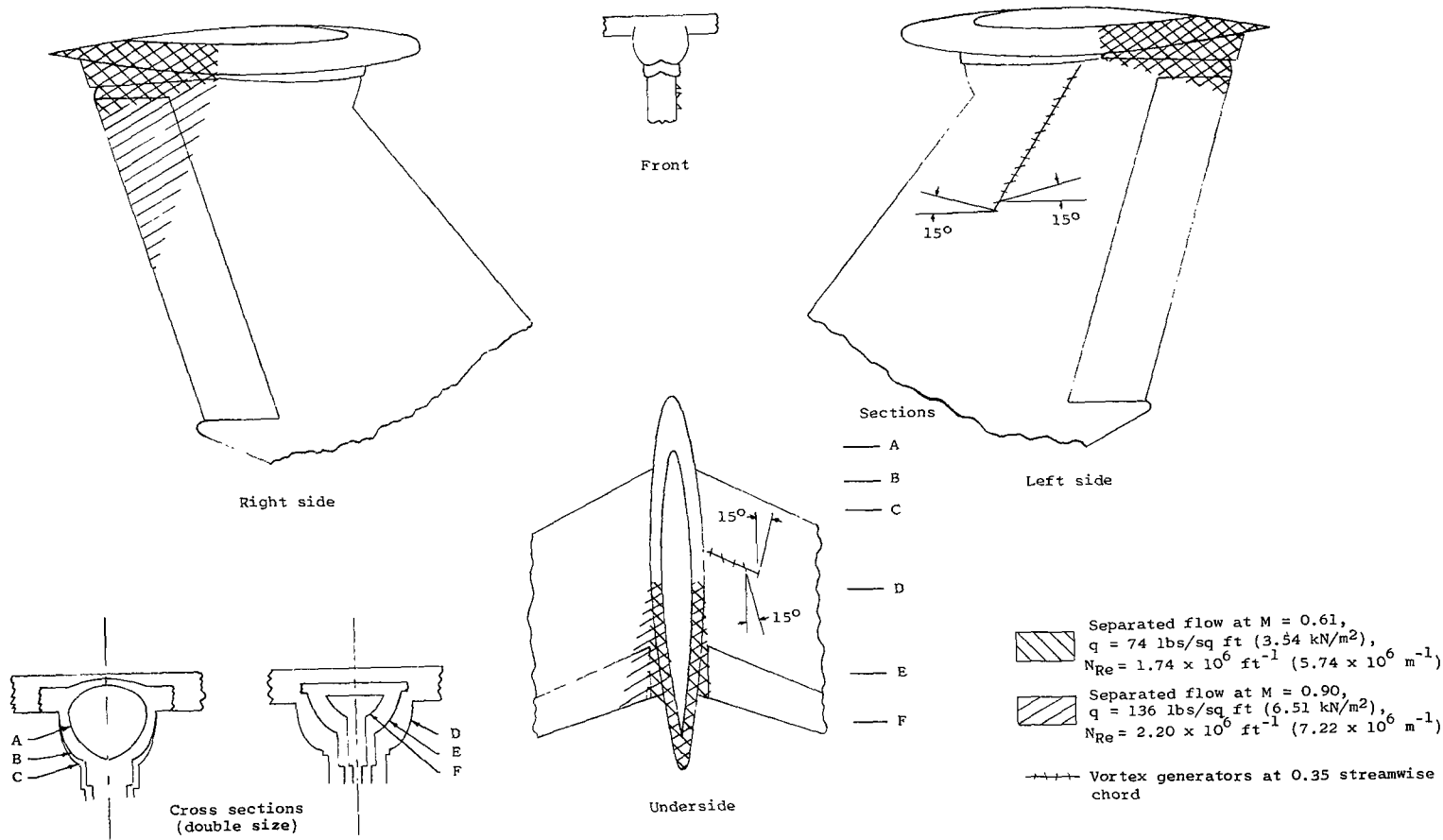
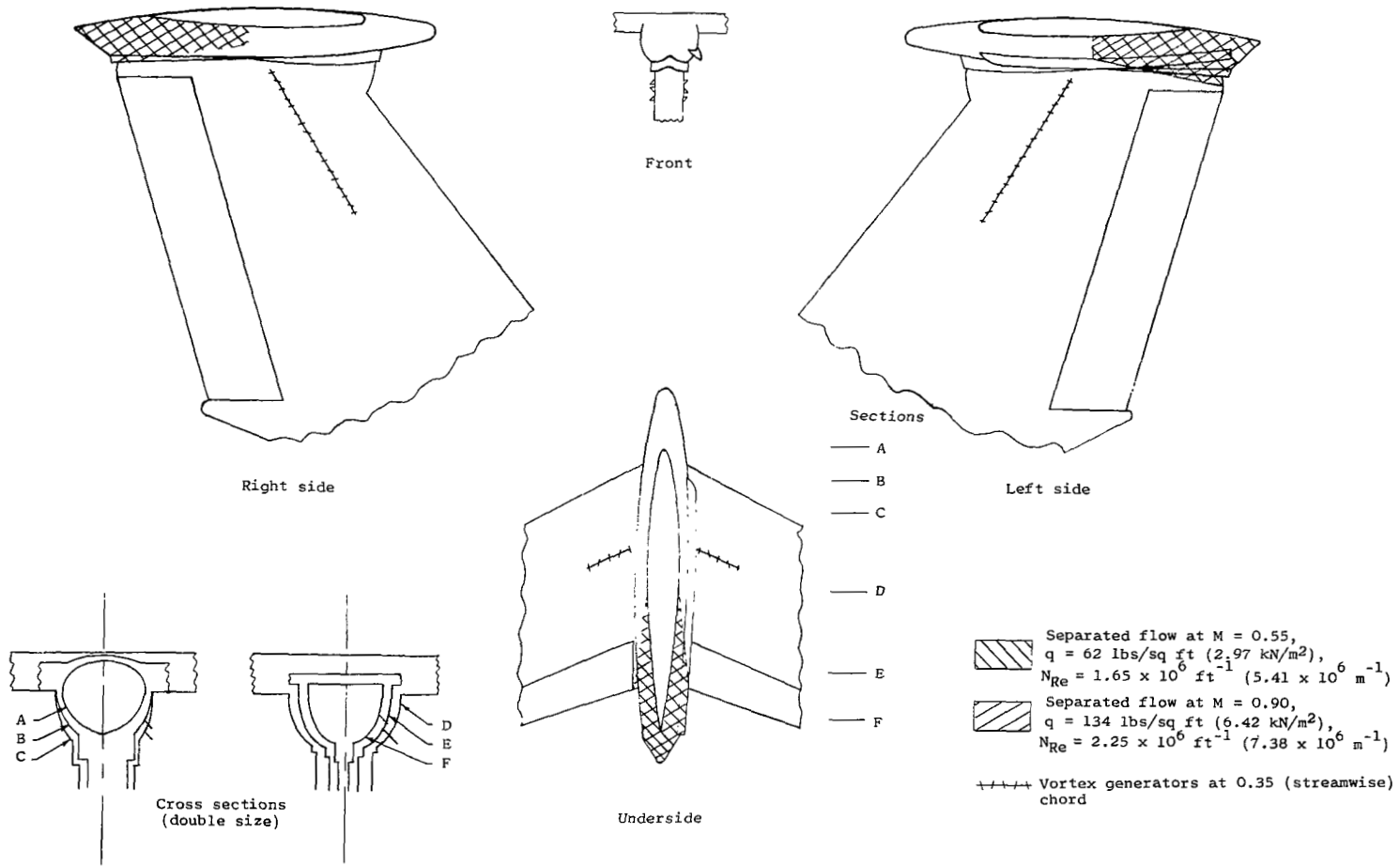


Figure 8.- Dynamic pressures, mass ratios, and Mach numbers covered for design configurations in freon.



(a) Bullet fairing 1 (original) with and without vortex generators.

Figure 9.- Bullet-fairing configurations and separated-flow regions.



(b) Bullet fairing 2 with vortex generators with and without fence.

Figure 9.- Concluded.

05U 001 27 51 3DS 00903
AIR FORCE WEAPONS LABORATORY/AFWL/
KIRTLAND AIR FORCE BASE, NEW MEXICO 87117

ATT MISS MADELINE F. CANOVA, CHIEF TECHNIC
LIBRARY /WLIL/

POSTMASTER: If Undeliverable (Section 158
Postal Manual) Do Not Return

"The aeronautical and space activities of the United States shall be conducted so as to contribute . . . to the expansion of human knowledge of phenomena in the atmosphere and space. The Administration shall provide for the widest practicable and appropriate dissemination of information concerning its activities and the results thereof."

—NATIONAL AERONAUTICS AND SPACE ACT OF 1958

NASA SCIENTIFIC AND TECHNICAL PUBLICATIONS

TECHNICAL REPORTS: Scientific and technical information considered important, complete, and a lasting contribution to existing knowledge.

TECHNICAL NOTES: Information less broad in scope but nevertheless of importance as a contribution to existing knowledge.

TECHNICAL MEMORANDUMS: Information receiving limited distribution because of preliminary data, security classification, or other reasons.

CONTRACTOR REPORTS: Scientific and technical information generated under a NASA contract or grant and considered an important contribution to existing knowledge.

TECHNICAL TRANSLATIONS: Information published in a foreign language considered to merit NASA distribution in English.

SPECIAL PUBLICATIONS: Information derived from or of value to NASA activities. Publications include conference proceedings, monographs, data compilations, handbooks, sourcebooks, and special bibliographies.

TECHNOLOGY UTILIZATION PUBLICATIONS: Information on technology used by NASA that may be of particular interest in commercial and other non-aerospace applications. Publications include Tech Briefs, Technology Utilization Reports and Notes, and Technology Surveys.

Details on the availability of these publications may be obtained from:

SCIENTIFIC AND TECHNICAL INFORMATION DIVISION
NATIONAL AERONAUTICS AND SPACE ADMINISTRATION

Washington, D.C. 20546